Conformable polyimide-based μECoGs: Bringing the electrodes closer to the signal source

Maria Vomero, Maria Francisca Porto Cruz, Elena Zucchini, Francesca Ciarpella, Emanuela Delfino, Stefano Carli, Christian Boehler, Maria Asplund, Davide Ricci, Luciano Fadiga, Thomas Stieglitz

PII: S0142-9612(20)30424-5

DOI: https://doi.org/10.1016/j.biomaterials.2020.120178

Reference: JBMT 120178

To appear in: *Biomaterials*

Received Date: 19 February 2020

Revised Date: 1 June 2020

Accepted Date: 5 June 2020

Please cite this article as: Vomero M, Porto Cruz MF, Zucchini E, Ciarpella F, Delfino E, Carli S, Boehler C, Asplund M, Ricci D, Fadiga L, Stieglitz T, Conformable polyimide-based μECoGs: Bringing the electrodes closer to the signal source, *Biomaterials* (2020), doi: https://doi.org/10.1016/j.biomaterials.2020.120178.

Credit Author Statement (according to CRediT roles)

Authors and their contributions:

Maria Vomero: Conceptualization, Data Curation, Formal Analysis, Investigation, Methodology, Project Administration, Visualization, Writing – Original Draft;

Maria Francisca Porto Cruz: Data Curation, Formal Analysis, Investigation, Methodology, Software, Writing – Contribution to Original Draft;

Elena Zucchini: Data Curation, Formal Analysis, Investigation, Methodology, Validation, Writing – Contribution to Original Draft;

Francesca Ciarpella: Data Curation, Formal Analysis, Investigation, Writing – Review &Editing;

Emanuela Delfino: Data Curation, Formal Analysis, Visualization, Writing – Review &Editing;

Stefano Carli: Validation, Visualization, Writing – Review & Editing;

Christian Boehler: Methodology, Writing – Review & Editing;

Maria Asplund: Methodology, Writing – Review & Editing;

Davide Ricci: Conceptualization, Methodology, Project Administration, Supervision, Visualization, Writing – Review & Editing;

Luciano Fadiga: Conceptualization, Funding Acquisition, Methodology, Resources, Scientific advice and supervision, Writing – Review & Editing;

Thomas Stieglitz: Conceptualization, Funding Acquisition, Resources, Scientific advice and supervision, Writing – Review & Editing.

Acknowledgements & Funding:

Part of this work was funded by the Cluster of Excellence BrainLinks-Brain-Tools (DFG, EXC1086). The authors would like to thank Ardavan Shabanian from the Laboratory for Design of Microsystems (IMTEK, University of Freiburg) for the technical support during the setting up of the Comsol model.

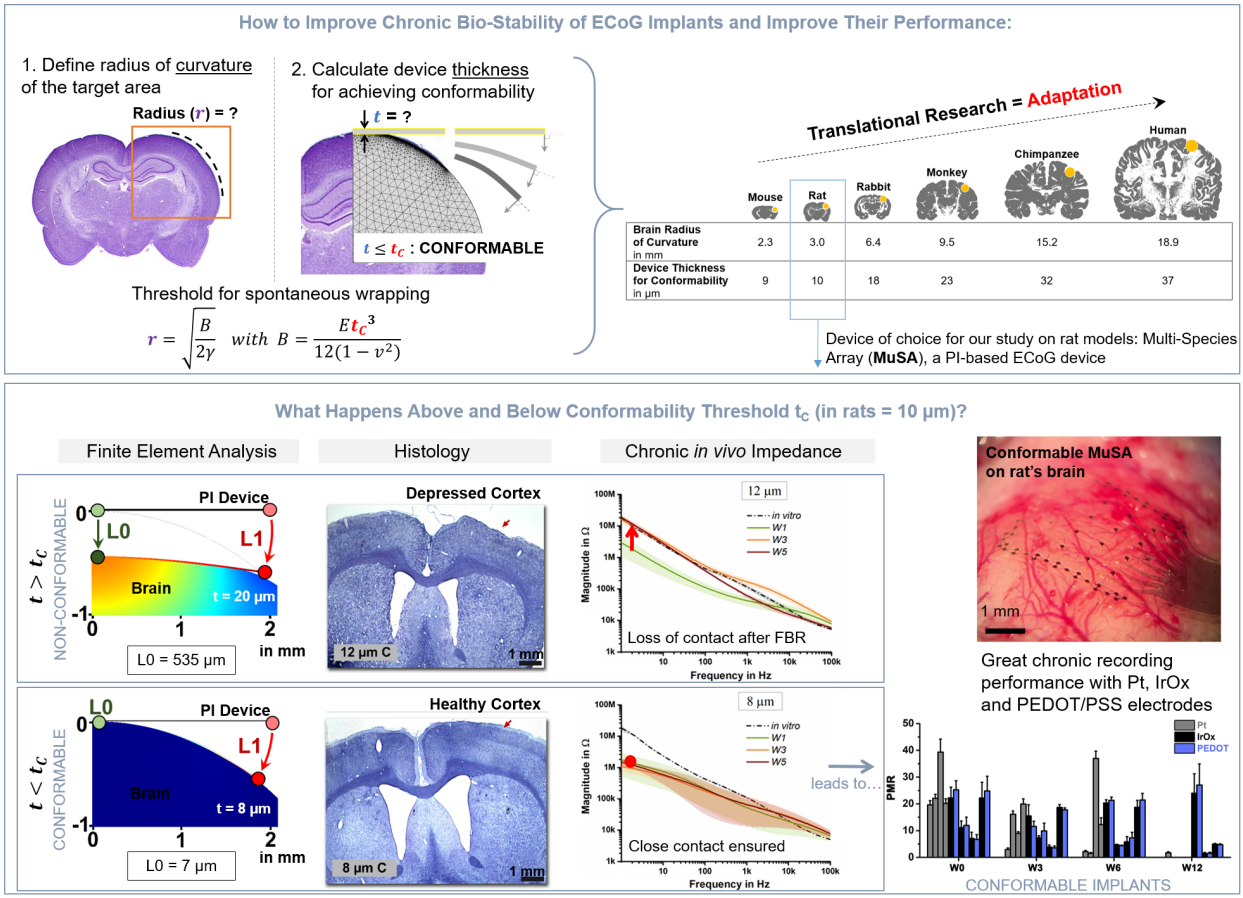
How to Improve Chronic Bio-Stability of ECoG Implants and Improve Their Performance:
1. Define radius of curvature of the target area
Radius (r) = ?
2. Calculate device thickness for achieving conformability
t = ?
t ≤ t_C : CONFORMABLE
Threshold for spontaneous wrapping
r = √(B/2γ) with B = Et_C³/12(1−v²)
Translational Research = Adaptation
Mouse
Rat
Rabbit
Monkey
Chimpanzee
Human
Brain Radius of Curvature in mm 2.3 3.0 6.4 9.5 15.2 18.9
Device Thickness for Conformability in µm 9 10 18 23 32 37
Device of choice for our study on rat models: Multi-Species Array (MuSA), a PI-based ECoG device
What Happens Above and Below Conformability Threshold t_C (in rats = 10 µm)?
Finite Element Analysis
Histology
Chronic in vivo Impedance
t > t_C
NON-CONFORMABLE
PI Device
L0
L1
Brain
t = 20 µm
L0 = 535 µm
in mm
Depressed Cortex
12 µm C
1 mm
12 µm
in vitro
W1
W3
W5
Magnitude in Ω
Loss of contact after FBR
Frequency in Hz
t < t_C
CONFORMABLE
PI Device
L0
L1
Brain
t = 8 µm
L0 = 7 µm
in mm
Healthy Cortex
8 µm C
1 mm
8 µm
Close contact ensured
leads to...
Conformable MuSA on rat's brain
1 mm
Great chronic recording performance with Pt, IrOx and PEDOT/PSS electrodes
Pt
IrOx
PEDOT
PMR
W0
W3
W6
W12
CONFORMABLE IMPLANTS

Conformable Polyimide-Based µECoGs: Bringing the Electrodes Closer to the Signal Source

Maria Vomero[a,b,c,*], Maria Francisca Porto Cruz[a,d], Elena Zucchini[d,e], Francesca Ciarpella[d,e,f], Emanuela Delfino[d,e], Stefano Carli[d], Christian Boehler[a,b], Maria Asplund[a,b,g], Davide Ricci[d,h], Luciano Fadiga[d,e], Thomas Stieglitz[a,b,i]

[a] *Department of Microsystems Engineering (IMTEK), University of Freiburg, Germany*
[b] *BrainLinks-BrainTools Center, University of Freiburg, Germany*
[c] *Currently at Department of Electrical Engineering (SEAS), Columbia University, New York City, USA*
[d] *Center for Translational Neurophysiology of Speech and Communication (IIT), Ferrara, Italy*
[e] *Section of Human Physiology University of Ferrara, Italy*
[f] *Currently at Section of Pharmacology, Department of Diagnostics and Public Health, University of Verona, Italy*
[g] *Division of Nursing and Medical Technology, Luleå University of Technology (LTU), Sweden*
[h] *Currently at University of Genova (DITEN), Italy*
[i] *Bernstein Center Freiburg, University of Freiburg, Germany*

Abbreviated Title*: Understand and Achieve Conformability with PI-Based ECoGs*

Authors' Contribution: MV: conceptualization, data curation, formal analysis, investigation, methodology, project administration, visualization, writing – original draft; MFPC: data curation, formal analysis, investigation, methodology, software, writing – contribution to original draft; EZ: data curation, formal analysis, investigation, methodology, validation, writing – contribution to original draft; FC: data curation, formal analysis, investigation, writing – review and editing; ED: data curation, formal analysis, visualization writing – review and editing; SC: validation, visualization, writing – review and editing; CB: methodology, writing – review and editing; MA: methodology, writing – review and editing; DR: conceptualization, methodology, project administration, supervision, visualization, writing – review and editing; LF: conceptualization, funding acquisition, methodology, resources, supervision, writing – review and editing; TS: conceptualization, funding acquisition, resources, supervision, writing – review and editing.

**email: mv2803@columbia.edu, postal address: Dept. of Electrical Engineering and Biomedical Engineering, Columbia University, CEPSR Building (room 911), 530 W 120th St, New York, NY 10027.*

Abstract

Structural biocompatibility is a fundamental requirement for chronically stable bioelectronic devices. Newest neurotechnologies are increasingly focused on minimizing the foreign body response through the development of devices that match the mechanical properties of the implanted tissue and mimic its surface composition, often compromising on their robustness. In this study, an analytical approach is proposed to determine the threshold of conformability for polyimide-based electrocorticography devices. A finite element model was used to quantify the depression of the cortex following the application of devices mechanically above or below conformability threshold. Findings were validated *in vivo* on rat animal models. Impedance measurements were performed for 40 days after implantation to monitor the status of the biotic/abiotic interface with both conformable and non-conformable implants. Multi-unit activity was then recorded for 12 weeks after implantation using the most compliant device type. It can therefore be concluded that conformability is an essential prerequisite for steady and reliable implants which does not only depend on the Young's modulus of the device material: it strongly relies on the relation between tissue curvature at the implantation site and corresponding device's thickness and geometry, which eventually define the moment of inertia and the interactions at the material-tissue interface.

Graphical Abstract (use color)

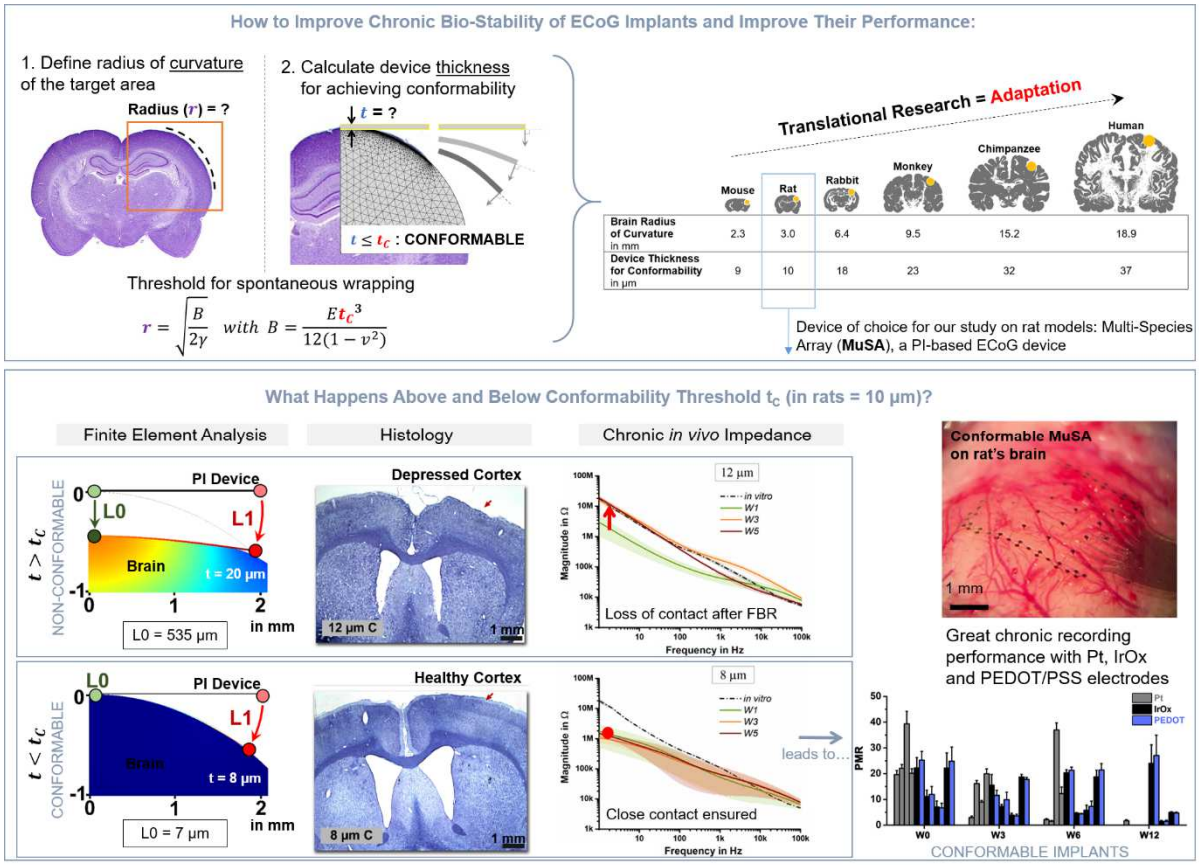

Keywords: *Polyimide-Based Electrocorticography Device; Bioelectronics; Conformability; Chronic Stability; Brain Recording; Tissue-Electrode Interface.*

Introduction

Skillfully engineered neural interfaces enable dynamic monitoring of brain signals and decoding of complex cognitive brain functions [1, 2]. Implantable bioelectronic devices are of substantial importance for neuroscience and contribute to a multitude of therapeutic solutions. Their role in the treatment of neurological disorders is growing in importance and a more wide-spread use of implantable bioelectronic devices is expected in the future. For acquiring high-quality neural data, it is crucial to ensure long term bio-stability of the implanted devices and to cause minimal tissue damage [3–5]. In contrast, the inflammatory and wound healing response to brain implants (*i.e.*, foreign body response or FBR) usually leads to their encapsulation and insulation from the neurons, a process extremely deleterious for the success of chronic studies [6, 7]. Therefore, it is desirable to lower – or ideally eliminate – the FBR to neural implants. The most efficient strategies to achieve this appear to be those addressing structural aspects of the implants. Experimental work has shown that reduced dimensions and minimized bending stiffness and rigidity have clear beneficial impact on the electrode-tissue interface [1, 8]. The mechanical interaction between

implants and surrounding tissue (known as structural biocompatibility) applies to both the initial device-tissue coupling and to their interactions over time, in terms of micro-movements and stress at the interface. When the mechanical mismatch between implants and neural tissue is reduced, the biotic/abiotic interface is stabilized and electrodes and electrically active cells remain in close contact. Thereby, the high-quality of the recorded signals can be sustained for longer periods [3, 5]. In regards to intracortical microelectrode arrays, for instance, it was shown that ultra-flexible and exceptionally small devices are able to perfectly integrate with the host tissue without inducing any scar formation [8]. A recent study also showed evidence that it is possible to record for 6 months from rat brains using up to 1024 active sites distributed on 48 polymer shanks without inducing severe brain damage [9]. The hypothesis that soft structures reduce tissue reactivity is indeed gaining support, together with the belief that flexible implants are more suitable for long-term studies because they are more reliable than their stiff (silicon-based) counterparts. Various polymers have been explored as alternatives to silicon as substrate materials. Among them, PDMS (polydimethylsiloxane) is the one with the lowest Young's modulus ($E < 1$ MPa) and it was demonstrated to be of great significance for subdural spinal cord implants, which involve highly sensitive and mobile structures [1]. Another frequently used polymer is polyimide (PI) that, despite being considerably stiffer than PDMS ($E \geq 1$ GPa), has gained importance as a biomaterial for implantable bioelectronics [10, 11]. PI is particularly appealing because of its high bio-chemical and thermal stability and the ease with which it can be photolithographically processed. Additionally, the use of adhesion promoters like silicon carbide (SiC) allows better integration of metal components onto inert PI substrates [5, 10, 12]. On the one hand, PDMS better matches the mechanical properties of the tissue while PI thin-film technology, on the other, is more versatile and allows the geometry of the device to be adapted with micrometre precision to the anatomical area of interest. Here, we suggest that the relative PI stiffness can be overcome by tuning the device geometry, so that the resulting structures conform to the curvature of the tissue and perfectly adhere to it. By adapting the geometry of the implant rather than compromising on the construction material, we propose a trade-off between device robustness and compliance to the implanted body. Although conformability is beneficial for various types of implantable neuroelectronic interfaces, we focus on proving this point using electrode grids for electrocorticography (ECoG) microelectrode-arrays as example. However, our results can be transferred to any other applications where planar electrodes have to match curved surfaces, for instance spinal cord, cochlea or retina.

ECoG micro-electrode arrays are less invasive than intracortical devices, and yet provide the signal quality and spatial resolution necessary for diagnostic purposes and to serve as part of BCI (brain-computer interface) tools [1, 13, 14]. Their popularity greatly increased after it

was demonstrated that spike-like activity - corresponding to intracortical action potentials, the main form of communication among neurons - can be detected from the surface of the brain [3, 15, 16]. Although surface electrodes usually do not disrupt the blood brain barrier, the mechanical mismatch between polymer-based ECoG arrays and soft brain tissue is still an unresolved challenge: long-term surface implants face glial cells activation, subsequent gliosis and encapsulation of the electrodes, as well as depression of the underlying tissue [1, 17]. Recent technologies have attempted to eliminate these effects and improve the mechanical and electrical tissue/electrode contact, facilitating high frequency recordings and chronic stability of the implants by using ultra-thin and highly fenestrated substrates. In practical terms, this translates into great conformal coverage over the convoluted brain surface, increased contact area between tissue and active sites and reduced substrate footprint, which allows the diffusion of soluble factors through the device and lowers the inflammatory response [3, 15, 18]. Nevertheless, thinner and open-architecture devices can be difficult to handle and often lack the mechanical robustness and reliability needed in chronic scenarios.

In this study, we followed an analytical approach to identify the key factors for increasing device conformability (here defined as percentage of device surface area contacting the brain) and applied them, in a tailored manner, to animal models for validating our findings. First, we calculated the critical thickness for achieving conformability with polyimide-based ECoG devices on a rat brain, based on the elasto-capillarity model. We then manufactured highly fenestrated implants of various thicknesses (below and above conformability threshold) and implanted them chronically. A finite element model was used to predict the depression of the brain cortex underneath conformable and non-conformable (*i.e.,* stiffer) chronic epidural implants. Finally, we demonstrated that multi-unit activity could be recorded over 12 weeks using the conformable devices and with the support of state-of-the-art electrode materials (Pt, IrOx, PEDOT/PSS). Our results indicate that device conformability is of the utmost importance to maintain healthy tissue underneath, and that the right mechanical properties substantially increase the quality of the recorded data. It is indeed possible to manufacture highly stable and conformable ECoG implants using standard thin-film technologies and without the need for bioresorbable stiffeners that may improve handling but might trigger unwanted tissue reactions, as long as the geometrical characteristics of the target anatomical area are taken into account.

Materials and Methods

Device Fabrication: The Multi-Species Array (MuSA) devices were fabricated using standard microlithography techniques in the cleanroom facility (ISO 5, according to ISO

14644-1) at the Department of Microsystem Engineering (IMTEK) of University of Freiburg. First, U-Varnish-S polyimide (PI, UBE Industries, Ltd, Japan) was spun on silicon wafers (at 3000, 4500 and 9000 rpm for achieving a thickness of 6, 4 and 2 μm, respectively). Then, tracks, connection pads and active sites were patterned with the high resolution image reversal photoresist AZ 5214 E (MicroChemicals GmbH, Germany). O_2 plasma (80 W, Plasma System 300-E, PVA TePla, Germany) was used to activate the surface, thus promoting adhesion for the metal, which was subsequently evaporated onto each wafer (300 nm of Pt, Univex 500 Electron-Beam Evaporator, Leybold GmbH, Germany). Lift-off to remove the excess of metal was done in acetone and, after it was completed, the same image reversal photoresist was used to pattern the active sites of the devices that were supposed to be coated with iridium oxide (IrOx). 100 nm of iridium followed by 700 nm of IrOx (obtained by introducing O_2 in the sputtering chamber of the machine UNIVEX 500, Leybold GmbH, Germany) were sputtered on the devices and the lift-off in acetone was repeated. O_2 plasma was again used to activate the surface of the wafers before a second PI layer was spun onto all of them. The positive photoresist AZ 9260 (MicroChemicals GmbH, Germany) was used as a masking layer for the opening of the contact pads and electrode sites and for setting the outlines of the devices. PI was finally etched using O_2 plasma in reactive ion etching (RIE) machine (STS Multiplex ICP, SPTS Technologies, United Kingdom) with a multi-step protocol (200 W first and 100 W after, time varying with PI thickness). The photoresist was stripped off in an acetone bath and the devices were mechanically peeled off the wafers using flat tweezers.

Assembly and Packaging: In order to interface the MuSA devices with the TDT headstage (Tucker Davis Technologies Inc, Florida, EUA) for the *in vivo* recordings, they had to be connected to a male Omnetics connector (A79022-001) matching the female counterpart of an interconnect ending with the TDT. The male connector was first soldered onto a ceramic board made by (1) cutting and pressing HTCC (high temperature co-fired ceramic) tape (44000, ESL ElectroScience, Pennsylvania, USA) at 27 MPa; (2) laser patterning the holes (through which the pins of the Omnetics are inserted) and outline of the board; (3) organic burnout at 550 °C and sintering at 1500 °C; (4) applying AgPd paste to the front side of the holes and removing the excess from the back side to ensure a homogeneous coverage of their inner walls; (5) firing at 850 °C and grinding both the front and back side. Once the connectors were soldered to one side of the ceramic boards, the MuSA devices were soldered on the other side and 2-component epoxy (epoxy 1 in Figure 1) was used to protect and insulate the solder joints. Another layer of epoxy (epoxy 2 in Figure 1) was used to fill eventual micro-gaps between the ceramic substrate and the connector.

PEDOT Deposition: PEDOT/PSS was deposited on a subset of the MuSA devices in an electrochemical process following a protocol previously described on IrOx electrodes to improve the stability of the coating [19, 20]. Prior to the polymer deposition, all probes were immersed in PBS (0.01 M) and electrochemically cleaned by means of cyclic voltammetry (-0.6 V / 0.9 V, 100 mV/s, 10 scans) to obtain a chemically well-defined IrOx surface. Subsequently, the probes were transferred to an aqueous electrolyte containing the monomer EDOT (0.01 M) and the dopant sodium-polystyrenesulphonate (NaPSS, 5 mg/ml). PEDOT/PSS coatings were potentiostatically deposited with an Autolab 302N potentiostat (Metrohm Autolab, Filderstadt, Germany) in a three electrode configuration (with an Ag/AgCl reference electrode and a large stainless steel counter electrode) at a potential of 0.9 V and using a polymerization charge density of 300 mC/cm^2.

Elasto-capillarity Model: The elasto-capillarity model was used to describe the wrapping of a flexible sheet of length l, width w and thickness h around a rigid cylinder of radius r coated with a thin layer of wetting liquid of surface tension γ (in air) [21, 22]. Wrapping occurs spontaneously when the amount by which the surface energy E_S is lowered is at least equal to the elastic bending energy E_E required.

$$E_S = \gamma w l \tag{1}$$

$$E_E = \frac{B w l}{2r^2} \tag{2}$$

with

$$B = \frac{E h^3}{12(1-\nu^2)} \tag{3}$$

Where B is the bending stiffness in N*m, E is the Young's modulus in Pa and ν is the Poisson's ratio (adimensional). By equating and rearranging the equations, the following condition can be deducted for the spontaneous wrapping of the sheet around the cylinder:

$$r \geq \frac{L_{EC}}{\sqrt{2}} \tag{4}$$

with

$$L_{EC} = \sqrt{\frac{B}{\gamma}} \tag{5}$$

Where L_{EC} is referred to as elasto-capillary length.

Finite Element Model: A simplified version of the µECoG-brain system was modelled and simulated in COMSOL Multiphysics (COMSOL Inc., Massachusetts, USA). The model was created in 2-dimensions under the solid mechanics module and studied under stationary conditions. The polyimide array area was modelled as a slender rectangle with a length of 2 mm and thickness h and the brain cortex as a quarter-circle with a radius of 3 mm. Both

bodies were assumed to be linearly elastic with a density ρ, Young's modulus E and Poisson's ratio *v*.

Table 1. Mechanical Properties of Polyimide and Rat Brain Used for Modelling

	ρ in kg/m^3	*E*	*v*
Polyimide	*1100*	*9 GPa*	*0.34*
Brain Cortex	*1027*	*1.75 kPa*	*0.40*

The length in the out-of-plane direction was defined as 4 mm (width of the actual array area). The left boundaries of both bodies were set as symmetric (the system was mirrored across x=0) and the bottom boundary of the cortex was fixed. Furthermore, a contact pair was defined between array and cortex, with the first being the source and the second the destination. A point load in the milli-Newton range was applied on the left-inferior corner of the probe and, in order to approximate the real loading due to surface tension and capillary action, the direction of the load was defined as perpendicular to the instantaneous tangent of the deflection curve. With respect to the mesh, the element size of the cortex was defined as gradually finer towards its surface, with the finest size being at least two times smaller than that of the array (maximum element size of 40 and 80 μm for the cortex and array, respectively). Initially, the thickness h of the μECoG array was set as the critical thickness h_c (estimated by the elasto-capillary model) and the magnitude of the load was increased until the probe conformed to the cortex. The conformability threshold was defined as the point at which 90% of the array's length contacts the cortex. The thickness of the array was then set to values lower and higher than h_c in order to investigate how conformability changes with thickness. For the cases in which the conformability threshold was not met, an extra load was applied on the probe in order to force more contact with the brain.

Electrochemical Impedance Spectroscopy *in Vitro* and *in Vivo*: Electrochemical impedance spectroscopy (EIS) measurements were performed to characterize small and large electrodes (10 and 100 μm in diameter, respectively). A Solartron 1287 potentiostat/galvanostat (Solartron Analytical, North Carolina, USA) was used in a three-electrode setup - with a Ag/AgCl (KCl 3 mol·l^{-1}) reference electrode, a standard platinum counter electrode (Pt-1800) and the electrode to be analysed as working electrode - to characterize the electrodes in phosphate buffered saline solution (PBS, pH 7.4, P3813, Sigma-Aldrich, Missouri, USA). The AC excitation voltage was set to 100 mV and its frequency swept from 1 Hz to 100 kHz.

In vivo impedances of chronically implanted electrodes were measured using potentiostat/galvanostat (Reference 600, Gamry Instruments, USA) in a two-electrode setup. Each electrode was referenced to a low impedance stainless steel screw inserted into the rats' skull and measurements were collected every week for the whole duration of the implants. During the impedance measurements, a sine wave (100 mV RMS amplitude) was imposed onto the open circuit potential while varying the frequency from 1 Hz to 100 kHz.

Surgical Procedures for the First Batch of Chronic Implants and Histology: To validate the analytical results obtained from the finite-element model, eight adult Long Evans rats (all males, 400-500 g) were implanted with devices of various thickness (see Table 2 for the breakdown on device specifications, number of rats implanted per device type, and number of brain slices used for the analysis and statistics), some of them being above and others below the conformability threshold. Five of the rats were implanted with MuSA devices (all hosting Platinum - Pt - electrodes) and three were implanted with another set of ECoG devices, 12 µm-thick and PI-based, with different footprint than the MuSAs but same % of holed area (about 17%) over solid PI substrate. They also differed from the MuSAs in the electrode material because they all hosted glassy carbon (GC) electrodes. However, the role of GC as an electrode material is discussed elsewhere [12] and it is not part of this study. The footprints of the two implant designs (MuSA and GC) are referred to as HD (highly distributed fenestration) and PD (poorly distributed fenestration), respectively. All the devices were manufactured following the protocol described in the *Device Fabrication* section, but the GC implants required the additional step of pyrolysis for making the GC electrodes [12], which does not interfere with the rest of the fabrication. The experimental plan was designed in compliance with the guidelines established by the European Communities Council (Directive 2010/63/EU, Italian Legislative Decree n. 26, 4/3/2014) and the protocol was approved by the Ethics Committee for animal research of the University of Ferrara and by the Italian Ministry of Health (authorization n 332/2015-PR).

The animals were anesthetized with a mixture of Zoletil (Virbac, France; 30 mg/kg) and Xylazine (Bayer, Germany; 5 mg/kg) administered intraperitoneally (i.p.). For the entire duration of the procedure, the depth of anaesthesia was monitored by testing the absence of hind limb withdrawal reflex and was maintained by additional intramuscular (i.m.) doses of anaesthetic. The anesthetized animals were then placed in a stereotaxic apparatus (David Kopf Instruments, USA) equipped with ear bars (Model 957 for small animals) and a ≈ 2 cm-long incision was made along the midline of the cranium. The underlying muscle and connective tissue were retracted to expose the skull and a craniotomy (≈ 6 × 6 mm^2) was performed in the parietal bone to expose the somatosensory cortex, identified according to vascular landmarks and stereotaxic coordinates [23]. Sterile saline solution was applied

while drilling to avoid any local heating and to keep the bone surface clean. The devices were placed over the dura mater in the primary somatosensory barrel field (S1BF, anatomical target of the elasto-capillarity model) and the surface of the implanted tissue was protected using Kwik-Sil silicone polymer (World Precision Instruments Inc, USA). To assess the influence of the headstage components on cortex depression, the implanted animals where divided into sub-groups featuring the presence (C) or the absence (NC) of connector and headstage. When performing NC-type implantations, the bare devices were carefully placed on the brain cortex and silicone polymer was used to protect the craniotomy area. The animals' skin was then sutured above the skull bone. Differently, for the C-type implantations, five stainless steel bone screws were inserted into the skull and the devices were fixed by the connector to a custom-made small protective chamber, fabricated with a 3D printer (Voxel8 Inc, USA). Finally, the C-type implants were cemented to the skull using dental acrylic (Jet Repair Acrylic, Lang Dental Manufacturing, USA) and the skin was sutured around the chamber and the cement (Figure 5A reports a sketch of the two implant types).

Six weeks after implantation, the animals were deeply anesthetized (mixture of Zoletil and Xylazine as for the surgical procedures) and then transcardially perfused with 300 ml 0.9% saline solution at room temperature, followed by 500 ml cold fixative solution of 2.0% paraformaldehyde, 1.25% glutaraldehyde, and 2.0% sucrose (all from VWR, USA), prepared in 500 ml 0.1 M sodium PBS (pH 7.4). Their brains were then removed, post-fixed overnight at 4°C, and placed in a 30% sucrose-buffered solution until they sank. The brains were frozen and sliced in 50 µm-thick coronal sections using a sliding microtome (SM2000 R; Leica Microsystems, Canada).

Table 2. *In vivo* experimental breakdown (use color)

Device Specifications			**Experimental Details**					
PI Thickness in µm	**PI Fenestration Type**	**Electrode Material**	**Implant Subgroup**	**N. of Implanted Rats**	**Histology (6 weeks)**	**N. of Brain Slices**	**Chronic Impedance**	**Chronic Neural Recordings**
12	PD	GC	C	3	Yes	42	Yes (6 weeks)*	Yes (6 weeks)*
12	HD	Pt	C	1	Yes	12	Yes (5 weeks)	No
12	HD	Pt	NC	1	Yes	12	No	No
8	HD	Pt	C	1	Yes	15	Yes (5 weeks)	No
8	HD	Pt	NC	1	Yes	11	No	No
4	HD	Pt	C	1	Yes	22	No	No
8	HD	Pt	C	4	No	N/A	Yes (12 weeks)	Yes (12 weeks)
8	HD	IrOx and	C	4	No	N/A	Yes	Yes

		PEDOT/PSS					(12 weeks)	(12 weeks)

*Data not shown in this manuscript

Red font (first row) refers to a non-MuSA design (used for comparative purposes)

Blue background (first 6 rows): 1st batch of implants

Tan background (last 2 rows): 2nd batch of implants

Cortex Depression Analysis: To investigate the mechanical compliance of the devices to the tissue, the brain sections were stained with Thionin (Sigma Aldrich, USA) and viewed under bright field illumination with an Olympus BX51 microscope (Olympus, USA) coupled with a CX9000 color video camera (MicroBrightField, USA) and the Neurolucida system (MicroBrightField, USA). Thionin-stained sections were acquired at 125× magnification and the images were post-processed and analysed using ImageJ software (developed at the National Institutes of Health, USA). An ImageJ plugin was used to draw a grid over the acquired images of the brain sections. The cortex depression was then calculated as the difference (D = Lctr - Lexp) between the distance from two fixed points of the control hemisphere (Lctr) and of the implanted hemisphere (Lexp). To cover the entire area below the array, in each brain section, the difference (D) was calculated at three different locations for both hemispheres. The significance of the data (P value < 0.05) was evaluated using one-way ANOVA followed by Tukey's post hoc test.

Second Batch of Chronic Implants for Neural Recordings and Sensory Stimulation: The recording capabilities of different electrode materials were investigated using an additional set of C-type implants. Specifically, eight adult Long Evans rats (all males, 400 - 500 g) were implanted with 8 µm-thick arrays (thus, conformable), four hosting Pt electrodes and four hosting Iridium Oxide (IrOx) and PEDOT/PSS electrodes (see Table 2 for the experimental breakdown). The surgical procedure for this second batch of implants followed the same protocol described in the *Surgical Procedures for the First Batch of Chronic Implants* section. On the implantation day (day 0) and every week for the first 6 weeks, as well as on week 12, neural signals were recorded from anesthetized and head-fixed rats. Impedance measurements were again collected weekly during this second batch of *in vivo* experiments. The animals were anesthetized with a mixture of Zoletil and Xylazine as for the surgical procedures. Data were collected using a Tucker Davis Technologies multi-channel recording system 3 (Tucker Davis Technologies, USA) including: the ZIF-Clip®headstage with unity (1X) gain, the RZ2 real-time processor and the PZ2-256 battery-powered preamplifier. In order to reduce electromagnetic noise, the experimental setup was placed in a Faraday cage. Data were digitized at a sample rate of 12,207 samples/s at 18-bit resolution and transferred from RZ2 processor to computer by fast fibre optic connection. As required by the single-ended headstage configuration, reference and ground pins of the

headstage were tied together and connected to a skull screw. The reference electrode on the arrays was disconnected.

To elicit the neural response of the rat barrel cortex, a vibrating system was used to produce a multi-whiskers deflection along the horizontal plane. Rats whiskers contralateral to the craniotomy were shortened and inserted in a Velcro strip attached to a rod moved by a shaker (Type 4810 mini shaker, Bruel & Kjaer, Denmark) controlled by a National Instruments board (Austin, USA). The deflection stimulus, consisting of a sine waveform of 12 ms duration and an amplitude coincident with whiskers deflection of 500 µm was repeated 60 times and separated from the others by a 4 s pause.

***In Vivo* Recordings Data Analysis:** Neural signal analysis for all the data collected along with the weeks was performed using the software NeuroExplorer® (Version 5.115, Nex Technologies, USA). In order to verify the consistency of the multi-unit activity recorded from the surface of the cortex with the peripheral stimulation, spike detection from ECoG raw signal was performed as follows: data were band-pass filtered between 200 Hz and 6 kHz (filter order 4), a -3-standard deviations threshold was set and no refractoriness period was assumed [16]. The detected spike times were then visualized by computing raster plots and the peri-event time histograms were calculated time-locking the data to the start of the whiskers stimulation. This analysis shows the conditional probability of a spike at time t_0+t on the condition that there is a reference event at t_0. For our purposes, t_0 was set at the start of the whisker stimulation and t was set to 5 ms long bins. Spikes/Sec normalization was obtained as follows:

$$\frac{n_{counts}}{n_{trials} \times t}$$

Where n_{counts} were the bin counts of the histogram and n_{trials} were the number of whiskers stimulations (specifically, n_{trials}=60).

Finally, in order to assess the chronic performances of the different electrode materials, Peak/Mean Ratio (PMR) was calculated as the histogram peak value divided by the background mean value (bins outside peak and trough) considering a time window going from 50 ms before and 200 ms after the stimulation. Data are presented as mean of all channels ± SEM (specifically, for each Pt rat n=16 and for each IrOx or PEDOT rat n=8) over the weeks for a total number of eight rats (four Pt rats and four IrOx and PEDOT rats). The Log(PMRgap) was calculated as the base 10-logarithm of the ratio between the PMR mean value of the small electrodes over the PMR mean value of the large electrodes at every recorded week of two representative rats (one Pt rat and one IrOx and PEDOT rat).

Results and Discussion

The *MuSA* [4] devices were designed to conform to the rat cortex and assembled to a custom-made board (Figure 1 and S1 in supplementary). Theoretically, it can be calculated and predicted that the ability of a thin-film device to conform to a convoluted body depends on factors like thickness, geometry, level of fenestration, wettability and stiffness of the substrate [1, 15, 18]. The higher the level of conformability, the closer the recording sites are to the target tissue, ultimately improving the quality of the recorded signal. The theoretical prediction was experimentally verified over 12-week long implants in rat models.

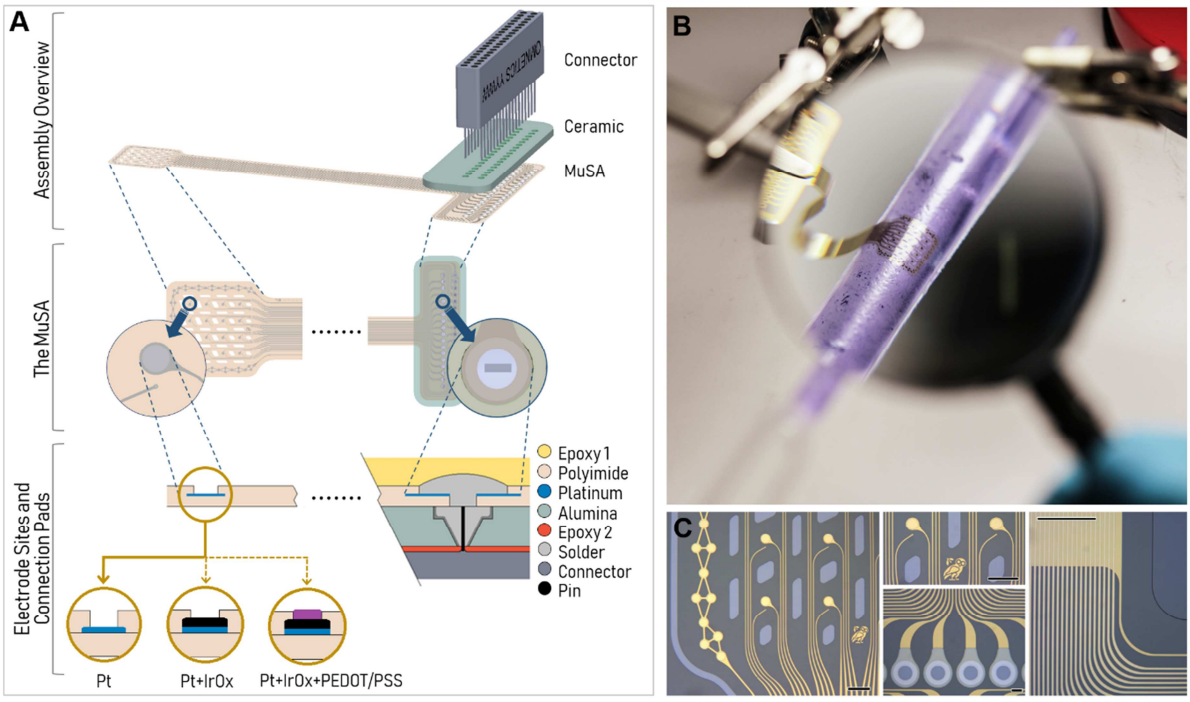

Figure 1. **Fabrication and Assembly of the MuSA**. (A) Schematic of the assembly of a 32 channel MuSA device to a fully custom-made ceramic board on which an Omnetics connector was soldered. 32 recording electrodes with diameter of 10 µm and 100 µm are distributed in a 4 x 4 array where each recording location is composed of an electrode couple (a large and a small electrode separated by 45 µm). Different versions of the MuSA have different electrode materials: Platinum (Pt), Iridium Oxide (IrOx) or PEDOT/PSS. (B) MuSA device wrapped around a pipette. (C) Microscopy images of some details of the MuSA device: electrode area, connection pads and interconnection tracks. Scale bars measure 200 µm. **Use color**

Elastocapillarity Model: To theoretically predict in which thickness range conformability could be expected, the mechanics of a thin-film polyimide (PI) substrate on the brain cortex was first studied with a general elasto-capillarity model. The model describes the wrapping of a flexible sheet of length *l*, width *w* and thickness *h* to a rigid cylinder of radius *r* coated with a thin layer of wetting liquid of surface tension γ (in air) [21, 22]. The wrapping of the sheet reduces the liquid-air interface by an area *w*l* (lowering the surface energy), at the expense of increasing its elastic energy due to bending. Therefore, for wrapping to occur

spontaneously, the amount by which the surface energy E_S is lowered must be at least equal to the required elastic bending energy E_E. Using Equation (4) (see materials and methods), it is possible to calculate the critical thickness for achieving the spontaneous wrapping of a PI foil around a curvilinear body with a given radius of curvature. Since the target anatomical area for this study was the primary somatosensory barrel field (S1BF) of Long Evans rats, a radius of curvature of 3 mm was used in the elasto-capillarity model [23]. Other parameters used to solve Equation (4) are: PI Young's Modulus of E = 9 GPa (information given by the supplier), PI Poisson's ratio of v = 0.34 [24] and cerebrospinal fluid surface tension of γ = 61 $mN \cdot m^{-1}$ [25–27]. The threshold value for conformability was found to be 10 µm. This means that 10 µm-thick PI implants should be able to naturally conform to the curvilinear rat brain only through elasto-capillary forces and without any additional pressure or further adhesive forces. Depending on the radius of curvature, and thus on the dimension of the target brain model under investigation, the thickness-threshold for achieving the conformability of a PI-based device can be determined using the same approach (see some examples in Figure 2). If to conform to a mouse brain a PI-based implant should not be thicker than 9 µm, such number becomes four times larger when conformability must be achieved on a human brain (Figure 2). This is, however, a gross approximation. While rodents are provided with an almost completely lissencephalic brain, primates are characterized by circumvolutions and gyri whose curvature radius is well below that of the global hemisphere. When gyri and sulci are subjected to investigation, considerations on the thickness for conformability of thin-film implants should be made using the radius of curvature estimated for those areas, specifically.

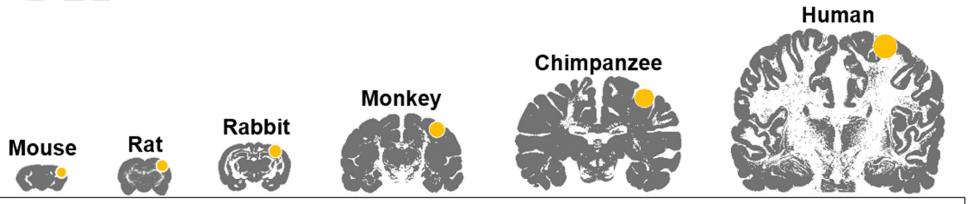

	Mouse	Rat	Rabbit	Monkey	Chimpanzee	Human
Brain Radius of Curvature in mm	2.3	3.0	6.4	9.5	15.2	18.9
Device Thickness for Conformability in µm	9	10	18	23	32	37

Figure 2. **Examples of different brain models with estimated radii of curvature** (corresponding to the yellow area in the drawings) and relative device thickness for conformability (calculated using the elasto-capillarity model and PI as device material). **Use color**

Finite Element Model & Analysis of Deflection: In order to better understand the process of conformability for a PI-based ECoG array onto the brain, the device/brain interaction was simulated via finite element modelling. The S1BF region was modelled as the cross section

of a cylinder with a radius of 3 mm and the array area of the device was represented as a rectangle of 2 mm x 4 mm. Both brain and device were assumed to be linearly elastic - because the expected deformation is negligible in comparison with the brain volume - and the simulation was solved for different PI thicknesses and mirrored across the y-axes (list of values and details found in materials and methods). At the initial state, the device was assumed to be in contact with the brain only in L0 (Figure 3A). A load was then applied on the array in L1 (other extremity or 'end' of the electrode array area), perpendicular to the instantaneous tangent of the deflection curve, until also L1 contacted the brain. The threshold case, represented by the 10 μm-thick PI ECoG array (Figure 3, middle), was used to determine the pressure necessary to bend the array until at least 90% of its surface area was in contact with the brain (referred to as contact pressure for conformability CP_c = 50 Pa). In the case of subthreshold devices (4 μm-thick), conformability was reached already by applying a pressure 5-folds smaller than CP_c, while to achieve the conformability of supra-threshold devices (20 μm-thick) an extra pressure was added to CP_c. After conformability was achieved, contact pressure (CP), contact area (CA) and brain depression (vertical displacement, VD) were calculated for the three cases (Figure 3B). The brain vertical displacement indeed increased with the device thickness. The 20 μm-thick PI array, as expected, did not reach conformability when CP_c was applied (only 37% of the array was in contact with the brain) but it needed an extra load of 167 Pa to conform to the cortex, which underwent a final vertical displacement of 535 μm. These results indicate that when PI-based ECoG devices are implanted, their ability to naturally integrate onto the tissue in a glove-like manner highly depends on their thickness. Non-conformable PI devices require force to adhere properly to neural tissue. Otherwise the peripheral electrodes tend to lose contact with the curved surface and cease to record. The external force applied to create the contact is transferred to the soft brain tissue that evidently deforms. Conformable devices are instead driven by surface tension and capillary forces to wrap around the curvilinear brain, inducing negligible brain displacement. They are not only easier to implant - because of the nature of the interaction with the brain - but also more reliable and prone to maintain the implantation position. This characteristic is undoubtedly important for brain mapping and spatial distribution analysis of the signal under investigation.

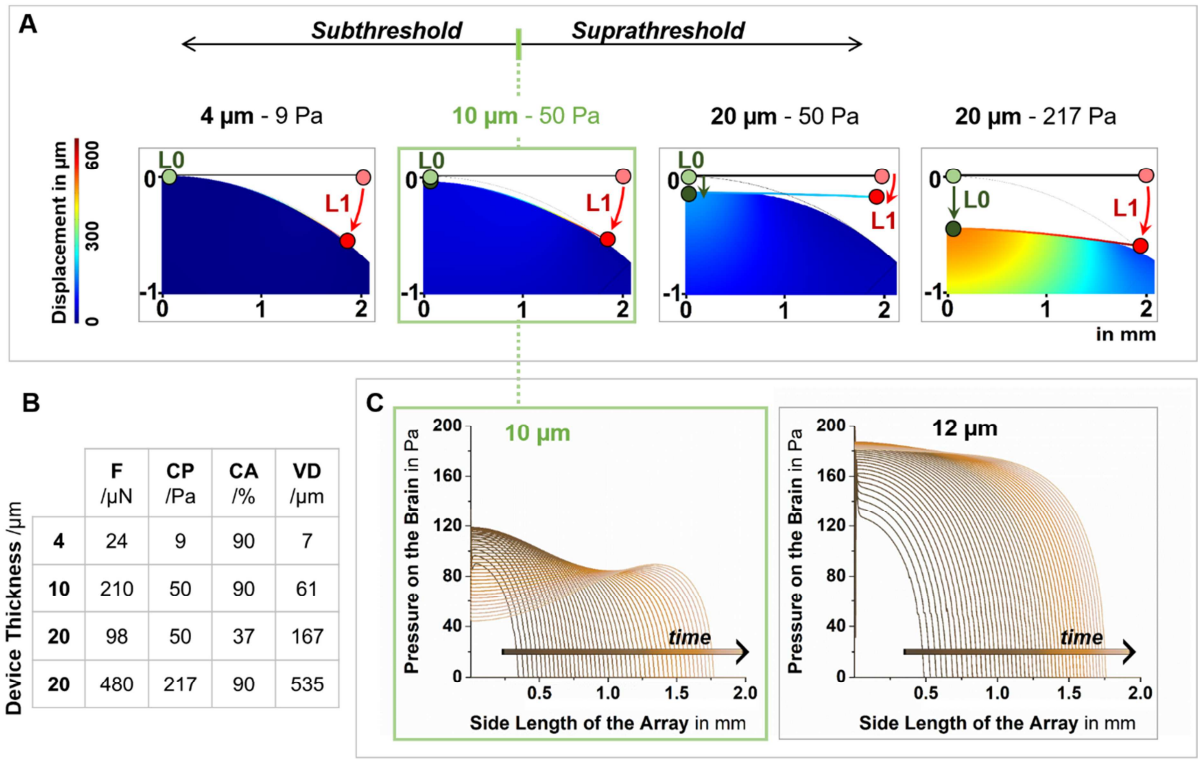

Device Thickness /µm	F /µN	CP /Pa	CA /%	VD /µm
4	24	9	90	7
10	210	50	90	61
20	98	50	37	167
20	480	217	90	535

Figure 3. **Device/Brain Interaction**. (A) Comsol model showing the vertical displacement of the rat cortex in contact with a polyimide sheet with different thicknesses (4, 10 and 20 µm) in L0 and subjected to a load F in L1. The load necessary to achieve conformability (90% or more of contact between brain a device and L1 lowered to the brain) and the vertical displacement of the brain are proportional to the thickness of the polyimide sheet. The 10 µm-thick device represents the threshold case (result from elasto-capillarity model) and therefore the force applied in this case to contact the brain can be referred to as Fc or Force for conformability. In the case of the 20 µm-thick device, an extra load had to be applied (in addition to Fc) to achieve sufficient contact with the brain. (B) Table listing load (F), contact pressure (CP), contact area (CA) and brain vertical displacement (VD) calculated by the model in the 3 cases. (C) Pressure distribution along the contact length from instant zero (dark brown) until conformability is reached (light brown) for 10 µm- and 12 µm-thick devices. **Use color**

The way a 10 µm-thick probe conforms to the brain - from the instant it comes in contact with it in L0 until nearly the entire electrode area adheres to it - can be understood by looking at the pressure change along the array side length over time (Figure 3C). The highest contact pressure value shifts and decreases during the simulation. At the final state, the contact pressure is higher towards the tip of the probe. Thicker probes (12 µm-thick, for instance) conform to the cortex only when an extra load is applied (otherwise conformability is not reached and the probe maintains its flat shape). For those probes, the pressure profile broadens and increases throughout the simulation, with the highest value being nearly constant along the contact length.

The finite element model implemented for this study does not account for substrate fenestration (*i.e*., number of holes in the PI) and metal layer but simplifies the array as a solid PI sheet. In reality, the electrode array area of the MuSA devices has a sieve-like design (see Figure S1 for the schematic), meaning that it is highly fenestrated (holes-to-solid PI ratio of 0.17) to allow the diffusion of fluids through the array and to reduce the amount of PI contacting the brain. According to plate theory, they are also more easily deflectable due to smaller equivalent width. On the other hand, the presence of the metallization layer on the neutral axis of the device should lead to an increase in stiffness, since the Young's modulus of Pt (the metal used here for the metallization of tracks) is almost 20 times higher than that of PI. Such increase, however, can be neglected for two reasons: first, the Pt-to-PI ratio is only 0.05 (while the ratio for fenestration is 0.17, as stated previously) and thus the metal is compensated by the presence of holes in the substrate; second, the thickness of the PI substrate is more than 30-folds larger than that of the metallization and - knowing that thickness raises bending stiffness to the third power - we can assume that the higher Young's modulus of the metallization is also compensated by the thickness of the PI.

***In vivo* impedance:** *In vivo* analysis was performed in two Long Evans rats using sub-threshold (*i.e.,* conformable, 8 µm-thick) and supra-threshold (or non-conformable, 12 µm-thick) MuSA devices, whose electrode impedance was monitored for 5 weeks. Before implantation, as expected, all electrodes had similar impedance (nearly 430 kΩ at 1 kHz for electrodes with diameter of 100 µm, see Table S1 in supplementary for details), independently from the thickness of the device to which they belonged (*in vitro* curve in Figure 4, for instance, shows the average impedance of four large Pt electrode in saline solution). After one week from implantation (Figure 4, W1 curve), the magnitude of the impedance of conformable and non-conformable electrodes was again comparable, probably due to a good initial tissue-electrode contact. At week 3, the impedance of the conformable electrodes remained overall the same but the impedance of the non-conformable ones increased significantly. This scenario was maintained until week 5 (Figure 4, W3 and W5). The behaviour of the phase angle followed the same trend: starting from week 3, it reached a steady-state in conformable implants while it had a non-stationary behaviour in non-conformable ones.

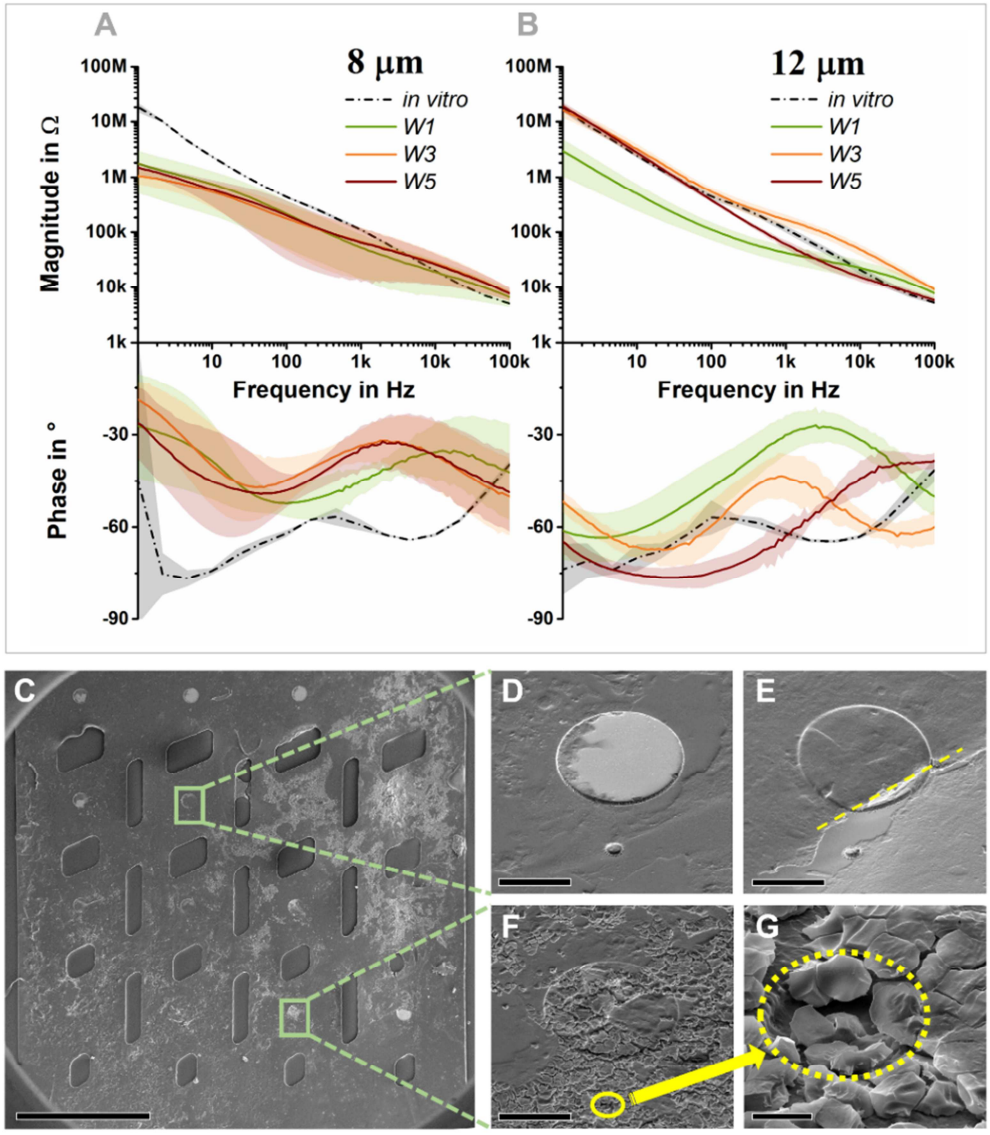

Figure 4. **Impedance as a tool to monitor the brain/tissue interface over time**. Bode plots (magnitude and phase) of 8 µm- (A) and 12 µm-thick (B) MuSA devices showing impedance measured *in vitro* (in PBS, 3 electrode-setup), and after 1, 3 and 5 weeks from implantation (in rats with a 2-electrode setup). The diameter of the Pt electrodes, in both cases, measured 100 µm. N=4 per electrode type. SEM images of an explanted MuSA device (12 µm-thick) after being implanted in a rat for 5 weeks: entire electrode area (C, scale bar = 1 mm), clean and intact couple of electrodes (10 and 100 µm in diameter) (D, scale bar = 50 µm), couple of electrodes nearby a "crease" (yellow dotted line in the picture) of the PI substrate (E, scale bar = 50 µm) which shows how the two electrode sizes are differently affected by a non-flat substrate: the larger electrode bends while the small electrode keeps its shape; electrode couple covered with biological substances and cells (F, scale bar = 50 µm) where the small electrode is basically entirely hidden by the cell debris (G, scale bar = 5 µm). **Use color**

The fact that impedance of electrodes belonging to non-conformable implants (12 µm-thick PI) increased over time could be ascribed to the type of interface they form with the

tissue: while the conformable device naturally adapts immediately to the curvilinear surface of the brain, the non-conformable device, although it is forced to adhere to it, does not tightly bind to the tissue but rather forcedly attach to it and tends to assume a more energetically favourable state over time (*i.e.*, it flattens and partially detaches from the brain). In the 8 µm-thick device case, electrodes seem to form a tight interface with the tissue and minimize the biotic/abiotic gap.

The explanted devices were optically inspected via scanning electron microscopy (SEM) before cleaning them. The entire electrode array area was covered by fibrotic tissue and blood cells (Figure 4C), as expected, although the electrode couples were still clearly visible underneath them (Figure 4 D-G). The device was unintentionally folded during the removal from the cortex (along the dotted yellow line in Figure 4E) and it was interesting to notice how the two electrode sizes are affected differently by the mechanical deformation of the substrate: while the large electrode deformed (and could eventually crack), the small electrode followed the curvature of the PI substrate but remained flat.

Histology: To validate the results obtained with the finite-element model simulation, the device conformability was also experimentally evaluated *in vivo*. MuSA devices of different thickness (4, 8 and 12 µm) were chronically implanted in rats for 6 weeks with the aim of quantifying the cortical depression (referred to as vertical displacement in the finite element model section) induced by their presence. Histological thionin staining clearly highlighted the effect of arrays with different degrees of conformability on the rat brains and facilitated evaluation of the biomechanical impact of the devices on the soft tissue in chronic scenarios (Figure 5B).

Two types of implantation procedures were adopted for comparison purposes: type C (connector: also used for impedance measurements) where the PI devices were soldered to a connector fixed on the skull using an acrylic cap, and type NC (no connector: only used for histology) for which the PI devices were implanted without connector and kept in place with a soft silicone-based polymer. For this type of implants (NC), no acrylic cap was used to seal the craniotomy and the external pressure exerted on the brain was considered negligible, as the only force was induced by the floating PI implants. The presence of the connector is necessary to create an electrical connection between implanted electrodes and recording system but it comes along with the need for a rigid cap or a support that keeps the connector in place and allows to access it during the recording sessions. Such supporting structure usually surrounds the craniotomy and might have an influence on the deformation of the brain. To decouple the depression induced by the PI implants from the depression induced by the acrylic cap, C and NC implants were carried out and analysed in parallel.

As for the computer simulation, the thickness threshold value for conformability seemed to lay within 8 and 12 μm also for the *in vivo* analysis. Indeed, no statistically significant differences existed between 4 and 8 μm-thick MuSA devices implanted with the headstage components (Figure 5A, 4 μm C and 8 μm C), while the depression caused by the 12 μm-thick MuSA device was significantly higher when compared to the 8 μm-thick MuSA values (Figure 5A, 12 μm C and 8 μm C). Moreover, when using sub-threshold devices (4 and 8 μm), physiological swelling of the brain (Figure 5B, 8 μm NC as an example of the phenomenon) out of the craniotomy borders was noticed. The swelling of the brain is a consequence of the surgical intervention and it is expected in any implantation. However, counter-pressure can be generated by the presence of non-conformable devices forced to adhere to the brain and by the headstage components. When the counter-pressure is bigger than the deformation caused by the swelling, the result is a depressed and flattened tissue (Figure 5B, 12 μm C and NC). When the implants are conformable, on the other hand, they do not flatten the brain but rather follow its curvature. Results also suggest that the presence of acrylic and connector clearly has an effect on conformable implants as well, and for implants below the conformability threshold (4 and 8 μm) it is the main cause of brain deformation (Figure 5A), potentially transferring forces via the interconnection cable [28]. Obtained data are in line with a previous study conducted by our group [12], where it had already been observed that a mild activation of the inflammatory response attributable to the chronic setup per se (*e.g.*, acrylic cap and screws) should be expected.

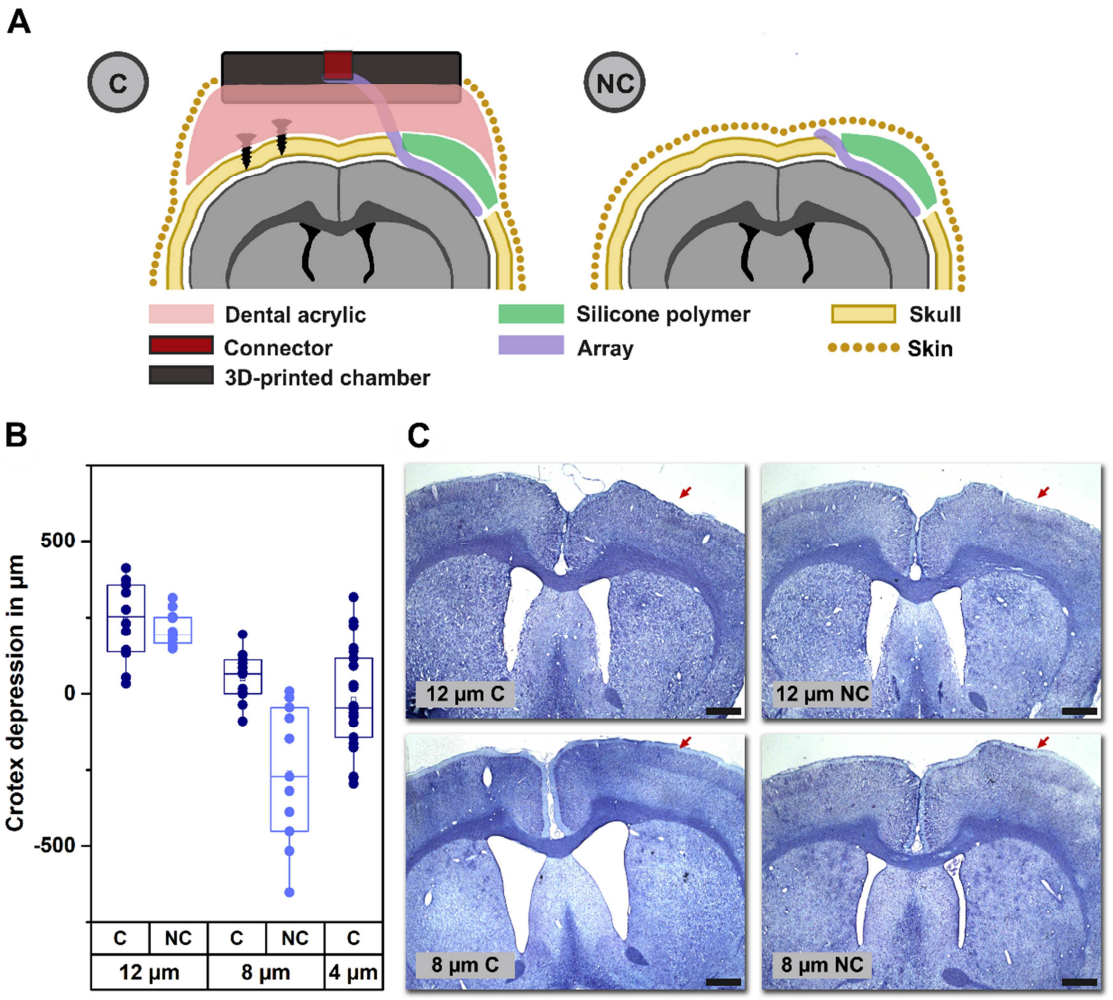

Figure 5. **Histology of the brain tissue**. (A) Schematic illustrating the setup used for two types of chronic implants: C, with connector and head-stage components mounted on the rat brain and NC, with device and silicone polymer only (NC); (B) Box plot with cortex depression values calculated from brains implanted with different-thickness MuSA devices, with and without connector and acrylic cap (C and NC, respectively); (C) Representative brain thionin-stained slices of supra and sub-threshold MuSA devices implanted for 6 weeks with and without connectors. Red arrows indicate the region of the tissue underneath the devices. Scale bar = 1 mm. **Use color**

Quantification of cortical depression was additionally performed on brains implanted for 6 weeks with 12 µm-thick PI-based ECoG devices with same percentage of fenestrated area over the solid PI substrate as for the MuSA devices (about 17%) but larger and less uniformly distributed fenestration holes within the electrode area ('poorly distributed fenestration', PD in Figure 6B). Histological results (Figure 6A) indicate that the brain depression greatly increases in case of devices with non-uniform fenestration when compared to all the other MuSA devices, conformable and non-conformable. Although they were fabricated using the same protocol and had same total thickness (12 µm), implants with non-uniformly distributed holes (PD in Figure 6B) caused significantly larger brain

depression than the one caused by the MuSA devices (with 'highly distributed fenestration', HD in Figure 6B). The negative depression values obtained for the PD devices can be linked to the swelling of the brain through the large fenestration holes. Thus, by designing a mesh-like or 'breathable' PI substrate, it is already possible to improve the tissue-electrode interface even of non-conformable implants.

Brain vertical depression values obtained from the finite-element model simulation and from the histological analysis post-implant are interestingly consistent (Table S2). In particular, the values calculated using supra-threshold devices (12 µm) are nearly identical: the simulation predicted 228 µm of brain displacement and the average value calculated via histology is 208 µm (± 10%). The finite-element simulation of the brain depression is closer to the real values when conformability is forced (hence, an extra load is applied for the device to adhere to the brain) because that is a rather 'controlled' force directly transferred onto the brain, which deforms proportionally to the force applied. In the case of threshold and subthreshold devices (10 µm or thinner), the brain depression obtained by the model only accounts for the mechanical mismatch between device and soft tissue, however *in vivo* the values are also affected by the presence of the head-stage components and by the fact that the brain inevitably swells due to the surgical procedure. Sub-threshold values are therefore difficult to model and predict with absolute precision because they are dominated by the type of setup used (C or NC) rather than by the device thickness. For the supra-threshold devices, however, the simplified finite-element model can be used to simulate the *in vivo* case when the PI implant under investigation has a hole/metal components ratio of about 3:1 over the entire electrode array area.

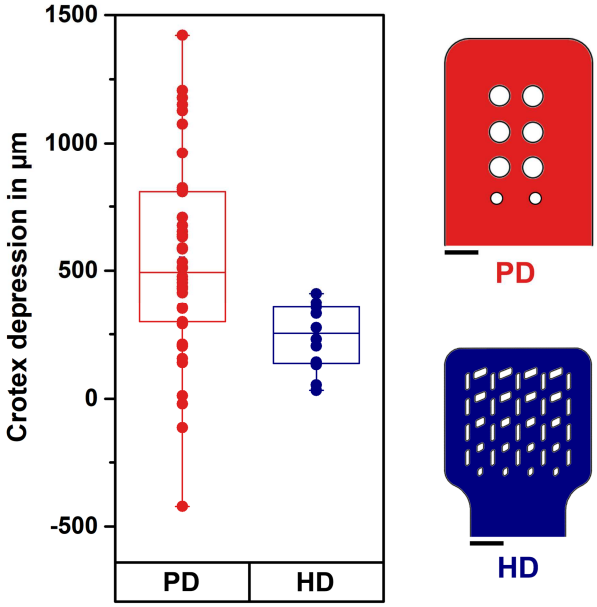

Figure 6. **Effect of device footprint on cortex depression**. Box plot showing cortex depression values calculated from brains implanted with a 12 µm-thick MuSA device with

highly fenestrated substrate (HD) and with a 12 µm-thick PI-based ECoG with poorly fenestrated substrate (PD). The solid/fenestrated area ratio was the same for both the devices (17% of holes over the PI area) and both implant types were performed using connectors and head-stage components (C-type). Scale bar = 1 mm. **Use color**

Chronic Impedance of Large and Small Electrodes: Additional chronic C-type implants were carried out using 8 µm-thick MuSA devices with different electrode materials (Pt, IrOx and PEDOT/PSS). For all three electrode materials it was observed that, starting from the first week after implantation, impedance of large (100 µm in diameter) and small (10 µm in diameter) electrodes belonging to the same couple (*i.e.*, with a pitch of 45 µm, as shown in Figure 1 and Figure S1) became basically indistinguishable. It should be noted that *in vivo* impedance was measured with a two-electrode setup using a distant skull screw as reference/counter electrode; it thus provided an estimation of conductivity of the path between reference and working electrode and it was influenced by the formation of fibrotic tissue around the implant. Between week 3 and week 6, the impedance of small electrodes was even lower than that of the large ones. The ΔZ, defined as difference between the logarithmic value of a small electrode impedance ($|Z_S|$) and of a large electrode impedance ($|Z_L|$) belonging to a couple, is the parameter used for interpreting the behaviour of the tissue-electrode interface over time (Figure 7A). This value was positive for the first 2 weeks and then became negative for all the electrode materials until week 12, when it reverted to positive. The ΔZ of the average difference in impedance of eight Pt electrode couples in the 1 Hz to 100 kHz frequency range is plotted in Figure 7B. Here, it is clear that the inversion from positive to negative starts at week 2 and mainly affects the impedance values measured at frequencies below 10 kHz. At frequencies higher than 10 kHz, the large electrodes always have lower impedance than the small ones, although the ΔZ value decreases drastically, even at high frequencies, between week 2 and week 6. This can be explained by associating the high-frequency behaviour of the impedance spectroscopy curve with the resistive component of a Randles equivalent circuit corresponding to the access resistance of the electrodes immersed in an electrolyte. At week 12, the overall situation reverted to the initial status, where the ΔZ value was positive in the entire frequency range. This scenario represents the majority of the chronic implants performed for this study (6 rats over 8 total). In two of the implants, the impedance of large and small electrodes over time did not follow a specific trend but was rather indistinguishable/superimposable after the second week from implantation. Although, theoretically, electrode impedance is highly dominated by the electrode area, after the first week in the brain, the geometric area of the implanted electrodes did not seem to have an influence on the measured *in vivo* impedance, which accounts for both electrodes and surrounding tissue. In the chronic implants performed in this study, the quality of the tissue-electrode interface did not entirely depend

on the electrode dimensions but it was rather determined by the coupling between tissue and electrodes and possibly by the formation of glia scar.

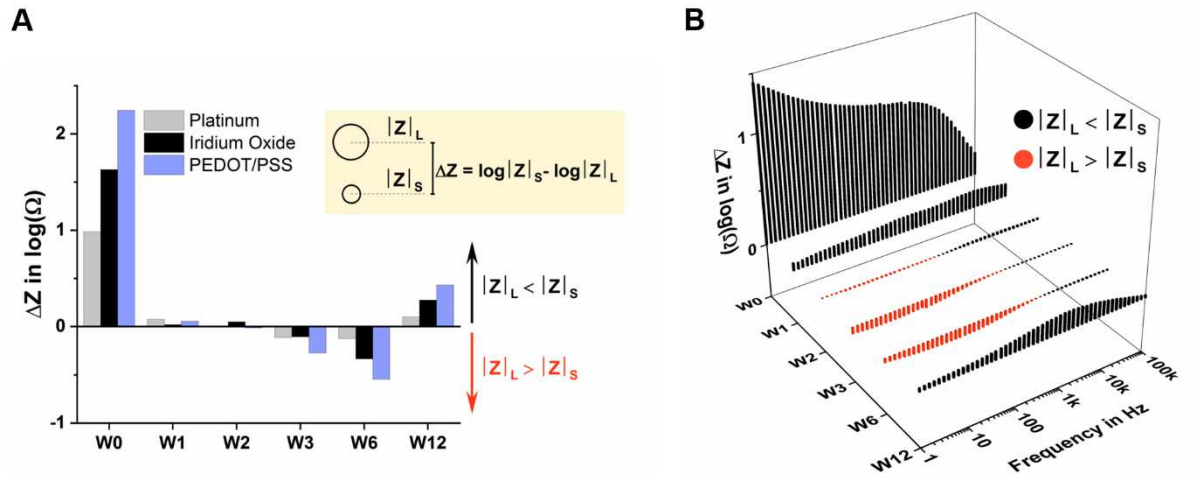

Figure 7. **Large v. Small Electrodes**. (A) Histogram showing the ΔZ - calculated as the difference between the logarithmic values of small ($|Z_S|$) and large electrode impedance ($|Z_L|$) belonging to a representative electrode couple, at 100 Hz - for 3 materials: Platinum (Pt), Iridium Oxide and PEDOT/PSS. (B) 3D plot showing the difference between the average (n=8) logarithmic impedance of small and large Pt electrodes over the whole frequency range (1 Hz to 100k Hz). In both (A) and (B) the ΔZ is plotted over 12 weeks of implantation. **Use color**

Chronic Recordings *in Vivo*: Chronic implants performed using 8 µm-thick MuSA devices with Pt, IrOx and PEDOT/PSS electrodes also served for studying the ability of different electrode materials to record in the long-term and test the overall stability of the implants. Ultra-conformable MuSA devices proved to perfectly adapt to the curvature of the S1BF rat cortex area and to establish a strong contact with the tissue (Figure 8A). Thanks to the adaptive and stable interaction occurring at the electrode-tissue interface, it was possible to both avoid cortical depression and neuronal loss and obtain high quality recordings. As already reported by Bockhorst and colleagues [16], high-frequency signals recorded from the surface of the brain correlate to the synchronous spiking of the neurons in the underlying cortical layers. This result comes with two main advantages: i) eliminates the need to insert the device into the cortical tissue (and therefore decreases the foreign body response) and ii) adds the possibility to map the high-frequency cortical activity of large brain areas while preserving the spatial resolution by using high-density µECoG devices. Indeed, the feasibility of resolving independent signals by using µECoG devices in humans and in animal models has been previously demonstrated [29–31]. Therefore, extending this achievement to higher frequency bands could bring new insights into the investigation of complex neural processes as well as great advantages in diagnostic and brain-machine interface applications.

Based on these findings, we verified the capability of the MuSA devices to detect multi-unit activity in chronic scenarios. Responses to sensory stimulation were recorded with different electrode materials (Pt, IrOx and PEDOT/PSS) and were explored during long-term implants on rat models. To better preserve the cortex and improve the tolerability of the implants, dura mater was left intact (devices were implanted epidurally) and, possibly thanks to the low thickness of this membrane in rats (~80 µm) [32], no repercussions on the detection of the high-frequency components were reported. Only the implants that lasted a minimum of 6 weeks (four rats with Pt electrodes and other four rats with IrOx and PEDOT/PSS electrodes) were considered for the analysis. Failures before this point were at the interconnection board level rather than at the device or electrodes. It should be noted that the end-date of the recording experiments does not correspond to the lifetime of the implanted electrodes. The MuSA devices were, in fact, still functioning when explanted. In order to evaluate the ability of the three electrode materials to discriminate burst-like activity triggered by the stimulation of the rats' whiskers, spikes were detected and peri-event time histograms were computed for all the recording sessions, time-locking the detected spike events to the start of the whiskers stimulation (see an example of the 6-week time-point in Figure 8B-C). When compared to Pt electrodes, IrOx (with or without the addition of PEDOT/PSS) demonstrated to be a more reliable and stable electrode material in the long-term (Figure 8D and S2 in supplementary). Moreover, IrOx and PEDOT/PSS were able to distinguish stimulus-dependent spikes from the ongoing activity with high Peak/Mean ratio values (PMR, see also materials and methods) at least up to 12 weeks. Some variability of the *in vivo* results can be attributed to different levels of anaesthesia, the inflammatory course and the intrinsic variability among animals. These factors substantially influence the overall performance of the implants but can hardly be managed. An overall drop in the recordings quality was observed with all the tested materials after 3 weeks but, in most cases, the quality of the recordings was restored after 6 weeks. This effect can be attributable to the different phases of the inflammatory response identified as acute (1-3 weeks) and chronic tissue reactions to the implanted devices [33].

Concerning the influence of the electrodes geometrical area (100 µm v. 10 µm) on their recording capabilities, significantly higher PMR values were reported for the large electrodes on the implant day, for all the electrode materials. However, consistently with the chronic impedance data shown in Figure 4, such a difference in the recording quality between large and small electrodes was settled along with the weeks in all rats and in some cases even reversed (Figure 8E).

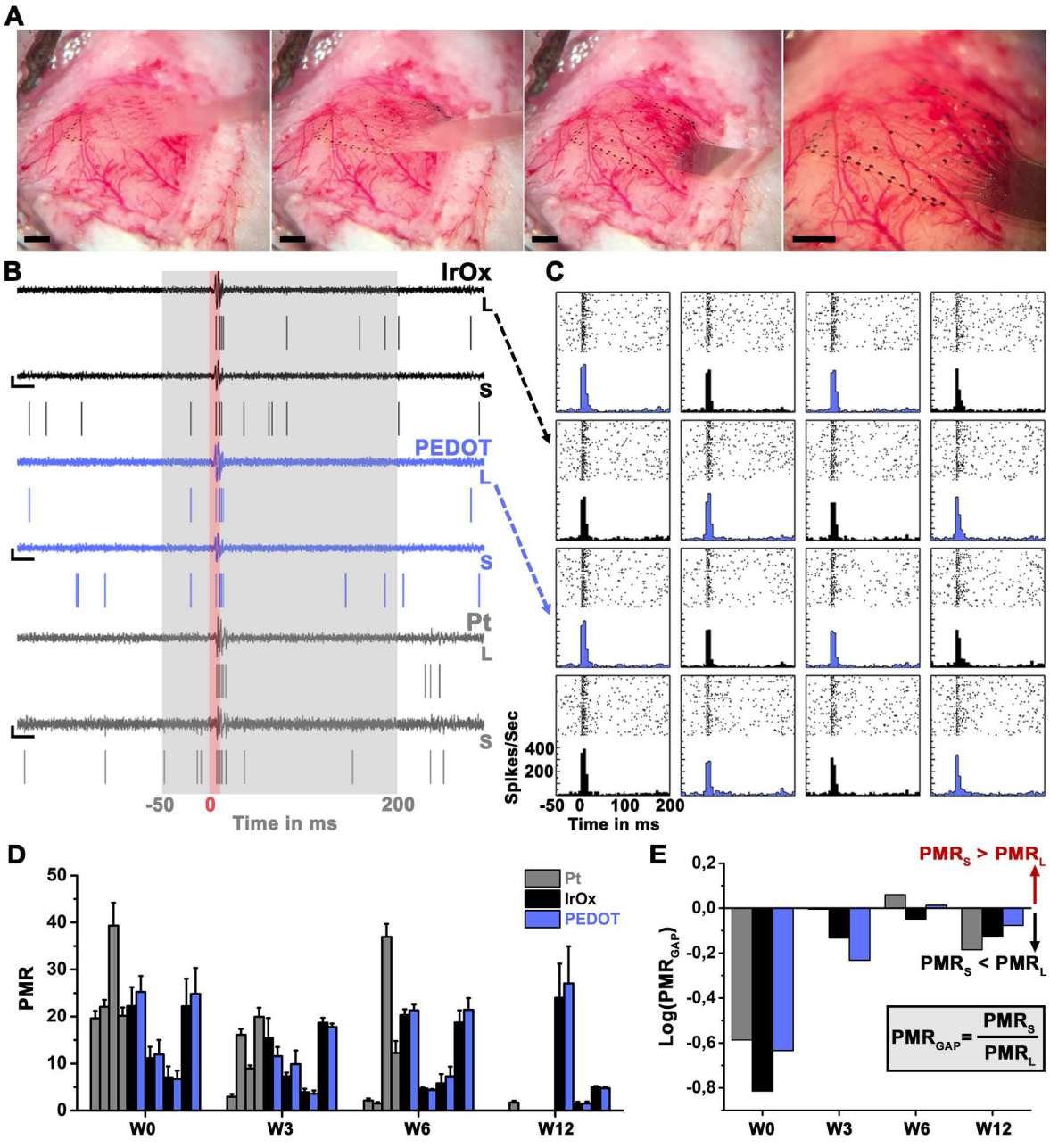

Figure 8. **High-Frequency Recordings**. (A) Sequence of pictures showing the conformable MuSA approaching the rat cortex. Scale bar = 1 mm. (B) Example high-pass filtered traces recorded after 6 weeks (200 Hz, large (L) and small (S) electrodes belonging to the same couple for the three tested materials) and corresponding spike rasters (scale bar 20 µV - 25 ms). Red background highlights the duration of the mechanical stimulation of the whiskers and in grey, the time window used for the Peak/Mean Ratio (PMR) calculation is shown. (C) Representative raster plots and peri-event time histograms of the large IrOx and PEDOT channels after 6 weeks from the implant day. (D) Plot of the PMR values of large electrodes (mean of all channels ± SEM, for each Pt rat n=16 and for each IrOx or PEDOT rat n=8) over the weeks for all the analysed rats (total number of rats=8, four Pt rats and four IrOx and PEDOT rats). Data belonging to the same rat are reported following the same order at each represented week. (E) Bar plot of the Log(PMR_{GAP}) calculated, as specified in the image, to compare the performances of large and small electrodes along with the weeks.

Representative data of one implant per type of electrode material are shown but such results were consistent in all the rats. Bar colours follow the same legend shown in D. **Use color**

Conclusion

PI-based devices represent the vast majority of thin-film implantable bioelectronic devices used in research nowadays. Although mechanically robust, chemically inert and biocompatible, PI is still much harder than the tissue it contacts. The mechanical mismatch between implant and implanted tissue can lead to the deterioration of the interface and progressive worsening of the electrical connection between artificial and biological ends. In the study presented here, the relation between probe design and quality of the tissue-electrode interface was investigated and an analytical approach was proposed to help optimizing the performance of PI-based ECoG implants in acute and chronic applications. The elasto-capillarity model was used to determine at which critical PI thickness elasto-capillarity forces are able to attract the device towards the target anatomical area without the need for 'external' pressure. This critical thickness varies depending on the radius of curvature of the cortical area of interest. In the case of electrocorticography devices, PI-based implants designed to be conformable to human brains can be 4 times thicker than conformable implants for mice. In our experience, conformability plays a key role during electrode placement and it helps maintain the device in place during the recording sessions. We saw that, when the implants are fully compliant to the brain, the tissue underneath them does not show significant depression nor deformation. Indeed, some depression was seen even in brain tissues implanted with conformable devices due to the connector and the head-stage components used to encapsulate the whole implant area. Interestingly, the brain depression values measured after 6 week-long implants are consistent with the values extrapolated from the finite-element model used to simulate the *in vivo* scenario. Long-term impedance measurements *in vivo* with conformable and non-conformable implants exhibited different behaviours: while the conformable implant formed a tight interface with the tissue which was maintained over time, the non-conformable implant at first seemed to follow the behaviour of the conformable one but, after 3 weeks, lost the tight connection to the tissue (its impedance gained about an order of magnitude).

Once we determined the critical thickness for achieving conformability on rat models, we performed additional chronic implants using only conformable devices and confirmed that the impedance measured *in vivo* gives information relative to the electrode/tissue interface as a whole rather than on the bare electrode site. Independent from the electrode material (Pt, IrOx or PEDOT/PSS), in fact, the impedance measured in sub-chronic and chronic

implants (2 to 6 weeks after implantation) does not depend on the electrode area but on the quality of the interface. Conformable devices proved to be able to detect peripherally stimulated high-frequency signals from the brain surface of rats for 12 weeks. Despite the volume conduction phenomenon, by tuning the design of ECoG devices, it is possible to bring electrodes closer to the signal source, eliminating the need of penetrating the brain for obtaining high-quality cortical recordings.

To summarize, the key factors for increasing the conformability to PI-based implants and their bio-stability over time are:

1. The thickness of substrate (PI): it should always be tailored to the specific animal model and anatomical area of the implant. Knowing the radius of curvature of such area, the device thickness for achieving conformability (t_c) can be estimated using the general elasto-capillarity model. The real thickness of an implant should be ≤ t_c.
2. The footprint of the device: an open architecture should be preferred to a solid one. At least 17% of the entire electrode area (*i.e.*, the area contacting the tissue) should be 'holed'. A fenestrated design helps the drainage of the fluids through the implant and promotes the growth of fibrotic tissue through the holes and around the device rather than in the space between tissue and active electrodes.
3. The distribution of the holes over the electrode area: a sieve-like design (many holes, highly distributed) conforms more uniformly than a semi-solid design (fewer holes, poorly distributed), even when the % of holes is comparable.
4. Holes-to-metal components ratio (3:1): the % of holes over the electrode area should be at least 3x higher than the % of surface occupied by the metal components (interconnects and electrodes). For this estimation we assumed a PI thickness at least 30x greater than the thickness of the metal layer.

Other important considerations can be made on the performance of different-diameter and material recording electrodes (when on a conformable substrate):

5. Recording electrodes with diameter ≤ 100 µm are expected to work similarly *in vivo* after 2 weeks from the implantation (end of acute inflammatory response), even if their electrical characteristics *in vitro* are different. Similar *in vivo* impedance values and comparable multi-spike recording capabilities can be expected, for instance, from 10 µm- and 100 µm-diameter electrodes.
6. Pt, IrOx and PEDOT/PSS are all valuable ECoG electrode materials capable of recording multi-spike activity. However, IrOx and PEDOT/PSS are indeed more reliable than Pt.

Highlights:

With this study, we have identified key factors for increasing the conformability to PI-based implants and their bio-stability over time. These are:

- The device thickness should be tailored to the target anatomical area;
- An open architecture footprint (sieve-like) should be preferred to a solid one;
- IrOx and PEDOT/PSS are reliable materials for chronic multi-spike recordings;
- Electrodes with diameter ≤ 100µm are expected to work similarly in chronic implants.

Acknowledgements & Funding: Part of this work was funded by the Cluster of Excellence BrainLinks-Brain-Tools (DFG, EXC1086). The authors would like to thank Ardavan Shabanian from the Laboratory for Design of Microsystems (IMTEK, University of Freiburg) for the technical support during the setting up of the Comsol model.

Supplementary:

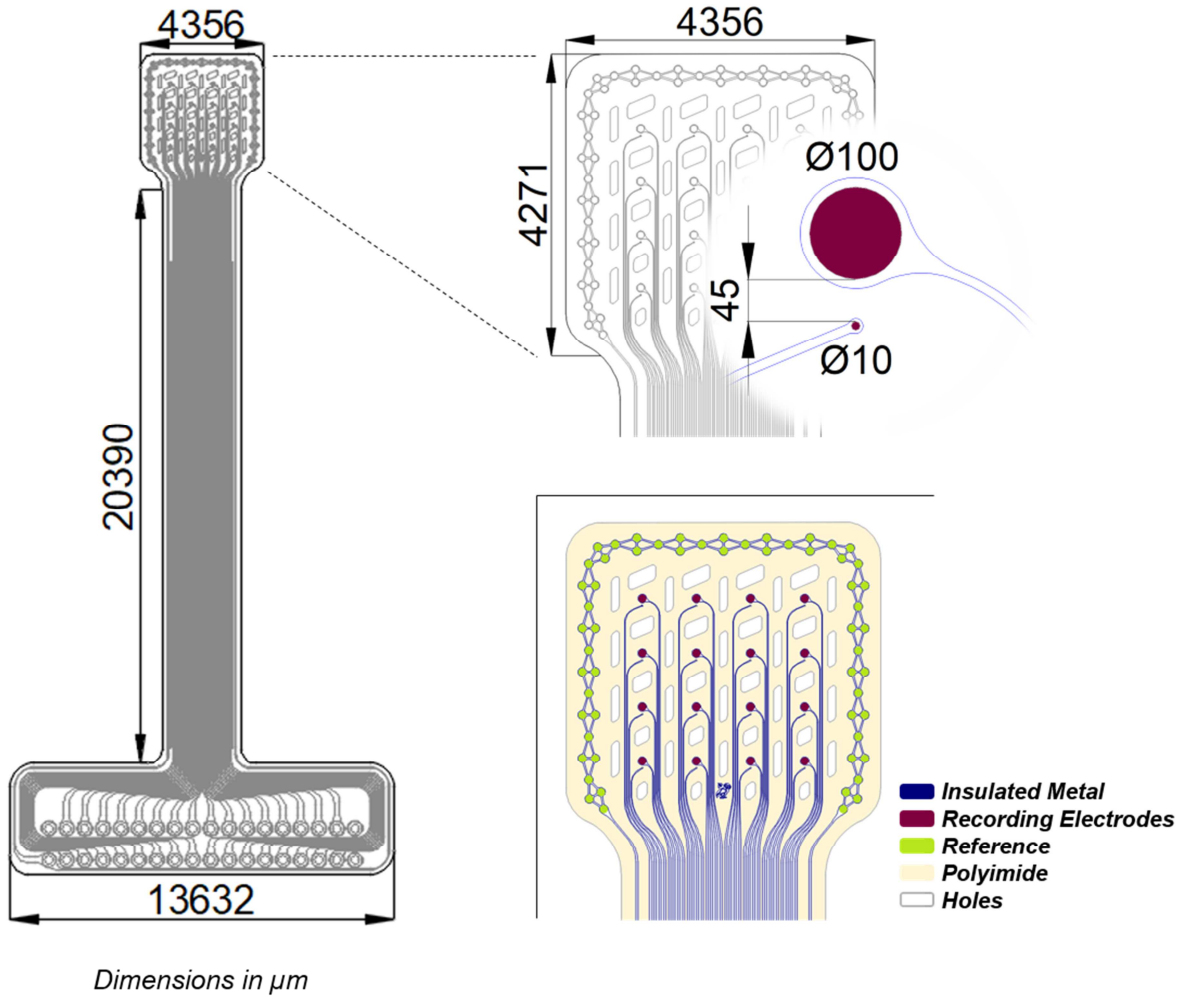

Figure S1. **Schematic of the MuSA** device with dimensions in µm.

Table S1. Average impedance values (measured at 1 kHz) of 100 µm-diameter Pt electrodes belonging to conformable (8 µm) and non-conformable (12 µm) PI substrate in PBS (in vitro row) and after one, three and five weeks from implantation in rats (W1, W3 and W5 rows).

Time Point	8 µm					12 µm				
	Mag		Pha		n	Mag		Pha		n
	Mean	SD	Mean	SD		Mean	SD	Mean	SD	
In vitro	4.28E+05	1.86E+04	-62.09	1.01	4	4.37E+05	5.97E+04	-56.87	5.56	4
W1	2.12E+05	1.60E+05	-52.32	4.34	8	1.11E+05	3.92E+04	-47.29	9.16	8
W3	1.75E+05	1.29E+05	-44.67	7.43	8	5.38E+05	1.01E+05	-59.65	8.08	8
W5	2.00E+05	1.68E+05	-48.05	5.47	8	3.75E+05	3.56E+04	-78.89	4.40	8

Table S2. Brain (vertical) depression values obtained with the finite-element model

simulation and with the histological analysis post-implant (data presented as the mean cortex depression value, n ≥ 12 for each type of device).

		Brain Vertical Depression in µm	
		Simulation	Histology
Thickness of the implant in µm	4	7	-20
	8	**19**	**-261**
	10	61	N/A
	12	**228**	**208**
	12 Non-Sieve	N/A	543
	20	535	N/A

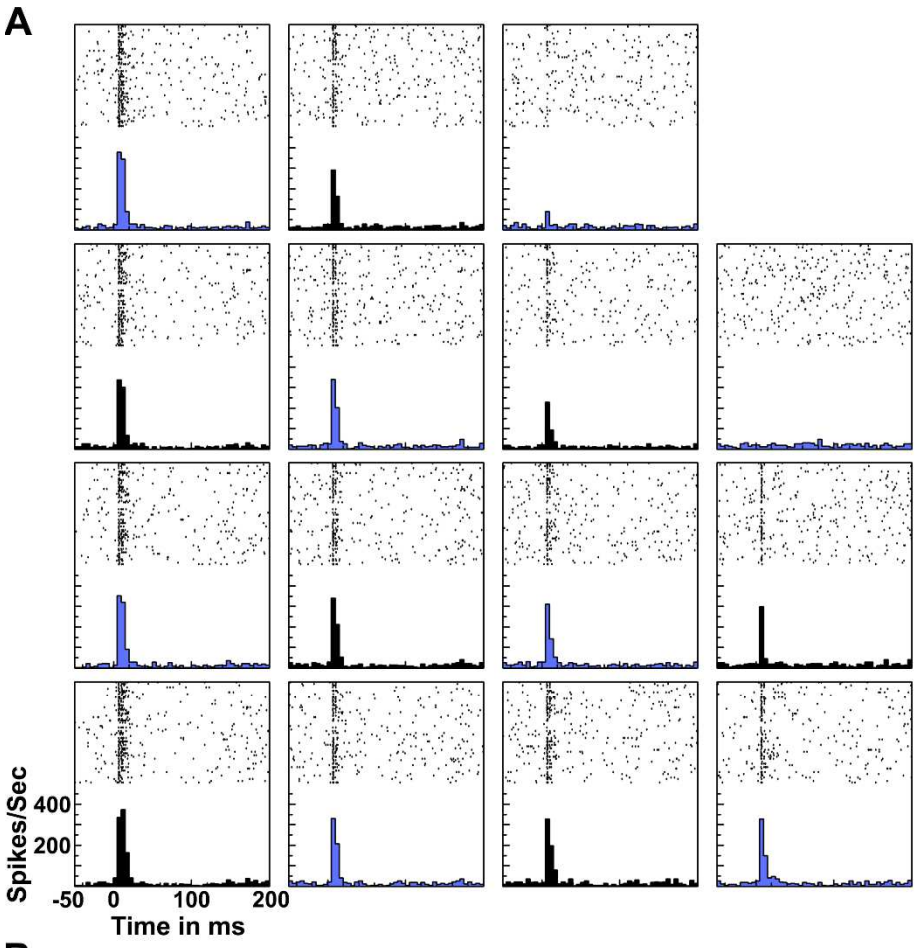

Figure S2. (A) Representative raster plots and peri-event time histograms of the small Iridium Oxide and PEDOT/PSS channels after 6 weeks from the implant day. Top right electrode was shorted to the disconnected reference electrode on the arrays. (B) Plot of the PMR values of the small electrodes (mean of all channels ± SEM, for each Pt rat n=16 and for each IrOx or PEDOT rat n=8) over the weeks for all the analysed rats (total number of rats=8, four Pt rats and four IrOx and PEDOT rats). Data belonging to the same rat are reported following the same order at each represented week.

References

[1] I. R. Minev *et al.,* "Biomaterials. Electronic dura mater for long-term multimodal neural interfaces," *Science (New York, N.Y.)*, vol. 347, no. 6218, pp. 159–163, 2015, doi: 10.1126/science.1260318.

[2] V. K. Mushahwar, D. F. Collins, and A. Prochazka, "Spinal cord microstimulation generates functional limb movements in chronically implanted cats," *Experimental neurology*, vol. 163, no. 2, pp. 422–429, 2000, doi: 10.1006/exnr.2000.7381.

[3] D.-H. Kim *et al.,* "Dissolvable films of silk fibroin for ultrathin conformal bio-integrated electronics," *Nature materials*, vol. 9, no. 6, pp. 511–517, 2010, doi: 10.1038/nmat2745.

[4] M. Vomero *et al.,* "Achieving Ultra-Conformability With Polyimide-Based ECoG Arrays," *Conference proceedings : … Annual International Conference of the IEEE Engineering in Medicine and Biology Society. IEEE Engineering in Medicine and Biology Society. Annual Conference*, vol. 2018, pp. 4464–4467, 2018, doi: 10.1109/EMBC.2018.8513171.

[5] M. Vomero *et al.,* "Glassy Carbon Electrocorticography Electrodes on Ultra-Thin and Finger-Like Polyimide Substrate: Performance Evaluation Based on Different Electrode Diameters," *Materials (Basel, Switzerland)*, vol. 11, no. 12, 2018, doi: 10.3390/ma11122486.

[6] V. S. Polikov, P. A. Tresco, and W. M. Reichert, "Response of brain tissue to chronically implanted neural electrodes," *Journal of neuroscience methods*, vol. 148, no. 1, pp. 1–18, 2005, doi: 10.1016/j.jneumeth.2005.08.015.

[7] S. M. Wellman and T. D. Y. Kozai, "Understanding the Inflammatory Tissue Reaction to Brain Implants To Improve Neurochemical Sensing Performance," *ACS chemical neuroscience*, vol. 8, no. 12, pp. 2578–2582, 2017, doi: 10.1021/acschemneuro.7b00403.

[8] L. Luan *et al.,* "Ultraflexible nanoelectronic probes form reliable, glial scar-free neural integration," *Science advances*, vol. 3, no. 2, e1601966, 2017, doi: 10.1126/sciadv.1601966.

[9] J. E. Chung *et al.,* "High-density, long-lasting, and multi-region electrophysiological recordings using polymer electrode arrays," 2018, doi: 10.1101/242693.

[10] J. Ordonez, M. Schuettler, C. Boehler, T. Boretius, and T. Stieglitz, "Thin films and microelectrode arrays for neuroprosthetics," *MRS Bull.*, vol. 37, no. 6, pp. 590–598, 2012, doi: 10.1557/mrs.2012.117.

[11] C. Hassler, T. Boretius, and T. Stieglitz, "Polymers for neural implants," *J. Polym. Sci. B Polym. Phys.*, vol. 49, no. 1, pp. 18–33, 2011, doi: 10.1002/polb.22169.

[12] M. Vomero *et al.,* "Incorporation of Silicon Carbide and Diamond-Like Carbon as Adhesion Promoters Improves In Vitro and In Vivo Stability of Thin-Film Glassy Carbon

Electrocorticography Arrays," *Adv. Biosys.*, vol. 2, no. 1, p. 1700081, 2018, doi: 10.1002/adbi.201700081.

[13] P. Jayakar, M. Duchowny, and T. J. Resnick, "Subdural Monitoring in the Evaluation of Children for Epilepsy Surgery," *J Child Neurol*, vol. 9, 2_suppl, 2S61-2S66, 1994, doi: 10.1177/0883073894009002091.

[14] N. J. Hill *et al.,* "Classifying EEG and ECoG signals without subject training for fast BCI implementation: comparison of nonparalyzed and completely paralyzed subjects," *IEEE transactions on neural systems and rehabilitation engineering : a publication of the IEEE Engineering in Medicine and Biology Society*, vol. 14, no. 2, pp. 183–186, 2006, doi: 10.1109/TNSRE.2006.875548.

[15] D. Khodagholy *et al.,* "NeuroGrid: recording action potentials from the surface of the brain," *Nature neuroscience*, vol. 18, no. 2, pp. 310–315, 2015, doi: 10.1038/nn.3905.

[16] T. Bockhorst, F. Pieper, G. Engler, T. Stieglitz, E. Galindo-Leon, and A. K. Engel, "Synchrony surfacing: Epicortical recording of correlated action potentials," *The European journal of neuroscience*, vol. 48, no. 12, pp. 3583–3596, 2018, doi: 10.1111/ejn.14167.

[17] P. Moshayedi *et al.,* "The relationship between glial cell mechanosensitivity and foreign body reactions in the central nervous system," *Biomaterials*, vol. 35, no. 13, pp. 3919–3925, 2014, doi: 10.1016/j.biomaterials.2014.01.038.

[18] A. A. Schendel *et al.,* "The effect of micro-ECoG substrate footprint on the meningeal tissue response," *Journal of neural engineering*, vol. 11, no. 4, p. 46011, 2014, doi: 10.1088/1741-2560/11/4/046011.

[19] C. Boehler, F. Oberueber, S. Schlabach, T. Stieglitz, and M. Asplund, "Long-Term Stable Adhesion for Conducting Polymers in Biomedical Applications: IrOx and Nanostructured Platinum Solve the Chronic Challenge," *ACS applied materials & interfaces*, vol. 9, no. 1, pp. 189–197, 2017, doi: 10.1021/acsami.6b13468.

[20] S. Carli, L. Casarin, G. Bergamini, S. Caramori, and C. A. Bignozzi, "Conductive PEDOT Covalently Bound to Transparent FTO Electrodes," *J. Phys. Chem. C*, vol. 118, no. 30, pp. 16782–16790, 2014, doi: 10.1021/jp412758g.

[21] J. Viventi *et al.,* "A conformal, bio-interfaced class of silicon electronics for mapping cardiac electrophysiology," *Science translational medicine*, vol. 2, no. 24, 24ra22, 2010, doi: 10.1126/scitranslmed.3000738.

[22] C. Py, P. Reverdy, L. Doppler, J. Bico, B. Roman, and C. N. Baroud, "Capillarity induced folding of elastic sheets," *Eur. Phys. J. Spec. Top.*, vol. 166, no. 1, pp. 67–71, 2009, doi: 10.1140/epjst/e2009-00880-4.

[23] G. Paxinos and C. Watson, *The rat brain in stereotaxic coordinates,* 6th ed. Amsterdam, Boston, Oxford: Academic, 2006.

[24] T. Boretius, D. Zimmermann, and T. Stieglitz, "Development of a Corrugated Polyimide-Based Electrode for Intrafascicular Use in Peripheral Nerves," in *IFMBE Proceedings, World Congress on Medical Physics and Biomedical Engineering, September 7 - 12, 2009, Munich, Germany*, R. Magjarevic, O. Dössel, and W. C. Schlegel, Eds., Berlin, Heidelberg: Springer Berlin Heidelberg, 2009, pp. 32–35.

[25] F. C. Hartman, G. M. LaMuraglia, Y. Tomozawa, and R. Wolfenden, "The influence of pH on the interaction of inhibitors with triosephosphate isomerase and determination of the pKa of the active-site carboxyl group," *Biochemistry*, vol. 14, no. 24, pp. 5274–5279, 1975, doi: 10.1021/bi00695a007.

[26] L. G. Ferren, R. L. Ward, and B. J. Campbell, “Monoanion inhibition and 35Cl nuclear magnetic resonance studies of renal dipeptidase,” *Biochemistry*, vol. 14, no. 24, pp. 5280–5285, 1975, doi: 10.1021/bi00695a008.

[27] E. K. Hodgson and I. Fridovich, “The interaction of bovine erythrocyte superoxide dismutase with hydrogen peroxide: inactivation of the enzyme,” *Biochemistry*, vol. 14, no. 24, pp. 5294–5299, 1975, doi: 10.1021/bi00695a010.

[28] J. Subbaroyan, D. C. Martin, and D. R. Kipke, “A finite-element model of the mechanical effects of implantable microelectrodes in the cerebral cortex,” *Journal of neural engineering*, vol. 2, no. 4, pp. 103–113, 2005, doi: 10.1088/1741-2560/2/4/006.

[29] I. Rembado *et al.,* “Independent Component Decomposition of Human Somatosensory Evoked Potentials Recorded by Micro-Electrocorticography,” *International journal of neural systems*, vol. 27, no. 4, p. 1650052, 2017, doi: 10.1142/S0129065716500520.

[30] X. Wang *et al.,* “Mapping the fine structure of cortical activity with different micro-ECoG electrode array geometries,” *Journal of neural engineering*, vol. 14, no. 5, p. 56004, 2017, doi: 10.1088/1741-2552/aa785e.

[31] N. Rogers *et al.,* “Correlation Structure in Micro-ECoG Recordings is Described by Spatially Coherent Components,” *PLoS computational biology*, vol. 15, no. 2, e1006769, 2019, doi: 10.1371/journal.pcbi.1006769.

[32] J. T. Maikos, R. A. I. Elias, and D. I. Shreiber, “Mechanical properties of dura mater from the rat brain and spinal cord,” *Journal of neurotrauma*, vol. 25, no. 1, pp. 38–51, 2008, doi: 10.1089/neu.2007.0348.

[33] A. Campbell and C. Wu, “Chronically Implanted Intracranial Electrodes: Tissue Reaction and Electrical Changes,” *Micromachines*, vol. 9, no. 9, 2018, doi: 10.3390/mi9090430.

Declaration of interests

☒ The authors declare that they have no known competing financial interests or personal relationships that could have appeared to influence the work reported in this paper.

☐The authors declare the following financial interests/personal relationships which may be considered as potential competing interests: